

A REDUCED ORDER CUT FINITE ELEMENT METHOD FOR GEOMETRICALLY PARAMETERIZED STEADY AND UNSTEADY NAVIER–STOKES PROBLEMS

EFTHYMIOS N. KARATZAS^{1,2}, MONICA NONINO², FRANCESCO BALLARIN²,
AND GIANLUIGI ROZZA²

ABSTRACT. We focus on steady and unsteady Navier–Stokes equations in a reduced order modeling framework. The methodology proposed is based on a Proper Orthogonal Decomposition within a levelset geometry description and the problems of interest are discretized with an unfitted mesh Finite Element Method. This work extends the approaches of [4, 27, 28] to nonlinear CutFEM discretization as well as to evolutionary in time fluid flow systems. We construct and investigate a unified and geometry independent reduced basis which overcomes many barriers and complications of the past, that may occur whenever geometrical morphings are taking place. By employing a geometry independent reduced basis, we are able to avoid remeshing and transformation to reference configurations, and we are able to handle complex geometries. This combination of a fixed background mesh in a fixed extended background geometry with reduced order techniques appears beneficial and advantageous in many industrial and engineering applications, which could not be resolved efficiently in the past.

keywords: Reduced Order Models; unfitted mesh; Cut Finite Element Method; Navier–Stokes equations; time dependent geometry.

1. INTRODUCTION

In the present work, we are interested in geometrically parametrized steady and unsteady Navier–Stokes equations in a Eulerian framework. We rely on an approach based on unfitted mesh Finite Element Method, which shows its flexibility especially when domains are subject to large deformations, and classical methods such as the Finite Element Method (FEM) fail.

In general, new computational tools have been invented and studied over the past years to solve numerically Navier–Stokes problems. The classical FEM is a powerful tool to discretize the physical domain of interest and simulate the behavior of the solution of the system, and its efficiency has been proven over the years, in a wide range of applications. Nonetheless, FEM capability to handle geometrically parametrized problems comes to a limit, this limit being given by extremely complex geometries, but also by situations where large deformations, fractures, contact points occur. As an alternative to classical FEM, we can consider Finite Element (FE) approximations of the physical fields that are not fitted to the actual physical geometry. The FE approximations are then cut at the boundaries and interfaces: this gives rise to the Cut Finite Element Method (CutFEM). For a more precise idea and for more rigorous definitions of what “cutting” a physical field means, and for a detailed introduction to CutFEM, we refer to [11] and references therein.

¹DEPARTMENT OF MATHEMATICS, SCHOOL OF APPLIED MATHEMATICAL AND PHYSICAL SCIENCES, NATIONAL TECHNICAL UNIVERSITY OF ATHENS, GREECE.

²SISSA, INTERNATIONAL SCHOOL FOR ADVANCED STUDIES, MATHEMATICS AREA, MATHLAB TRIESTE, ITALY.

E-mail addresses: karmakis@math.ntua.gr, mnonino@sisssa.it, fballarin@sisssa.it, grozza@sisssa.it.

2010 *Mathematics Subject Classification.* 78M34, 97N40, 35Q35.

The repeated solution of parametrized problems discretized by CutFEM is an expensive task (whose cost essentially depends on the size of the underlying background mesh), especially in complex geometries. It is precisely at this point that the Reduced Basis Method (RBM) comes into play. It is well known that the Reduced Basis Method is an extremely powerful tool to obtain a speedup in the simulation of the behavior of the solution of the system. The method relies on a set of already computed solutions (snapshots) for different parameter values: see, for example, [21, 22, 36]. Therein, these snapshots are FE approximations of the truth solution, thus the RBM relies on the FEM. Even though in general there are several methods that can be employed to project the full order system to a reduced system, see for example [14–16, 25, 31, 34], in the present work we will employ the Proper Orthogonal Decomposition (POD). We use a fixed background geometry and mesh: this approach leads to important advantages whenever a geometry deforms, [4], and it overcomes several related limitations in efficiency, compared with traditional FEM, see e.g. [6, 27, 29]. For the reader interested in Reduced Order Methods based on classical FEM we refer to: [22] for Proper Orthogonal Decomposition, to [14, 22, 25, 31, 34] for greedy approaches and certified Reduced Basis Method, to [14–16] for Proper Generalized Decomposition (PGD), to [20, 34] for linear elliptic and parabolic systems and to [19, 32, 44] for nonlinear problems.

The aim of this work is to implement a Reduced Basis Method for the stationary and evolutionary Navier–Stokes equations, that relies not on FEM but on CutFEM instead: already existing results on RBM applied to Navier–Stokes problems with standard FEM can be found for example in [23, 32, 40], as well as results concerning RBM based on embedded FEM for different kind of problems, see for example [27, 29], as well as [28] for Navier–Stokes with the Shifted Boundary Method. Our major goal is to apply this technique to CutFEM nonlinear fluid flow problems, but in order to do so, we test and study the procedure step by step: we first begin with the static parametrized steady Navier–Stokes equations, then we will move to the time-dependent parametrized fluid problem.

In Section 2 we first introduce the steady Navier–Stokes equations with incompressibility constraint in a fluid domain where the shape of some of the boundaries is described through a levelset function depending on a geometrical parameter; we move then to the unsteady Navier–Stokes equations, formulated over the same physical domain. Finally we focus on the unsteady Navier–Stokes equations in a domain, where the levelset function is now time-dependent, i.e. it changes with time. Afterwards, in Section 3 we present the reduced order approach for each of the aforementioned problems. Numerical results are described in Section 4 at both the high fidelity level and the reduced order level. Conclusions and perspectives are provided in Section 5.

2. FULL ORDER DISCRETIZATION BY CUTFEM

In this paragraph we introduce the problem formulation for the steady and unsteady Navier–Stokes equations. In the time-dependent levelset geometry test case, we assume that the deformation in time of the levelset geometry is given: this can be seen as a first step towards coupled problems in fluid dynamics, which we are not considering herein and which will be part of a future work. Let us now introduce some basic notions and definitions in the CutFEM framework: these definitions will be employed in the discrete formulation of the problems that we present hereafter.

2.1. CutFEM: an introduction to terminology and definitions. In the following we recall some definitions and terminology that are commonly used for Domain Decomposition techniques: Domain Decomposition is a useful tool that allows to tailor the approximation approaches to the different computational domains at hand.

Let Ω be the physical domain over which our problem is formulated, and let $\hat{\mathcal{T}}_h$ be a background mesh of mesh size $h > 0$ covering Ω . The *active mesh* \mathcal{I}_h and *active set of facets* \mathcal{F}_h are constituted by the background mesh elements T and facets F , respectively, that are

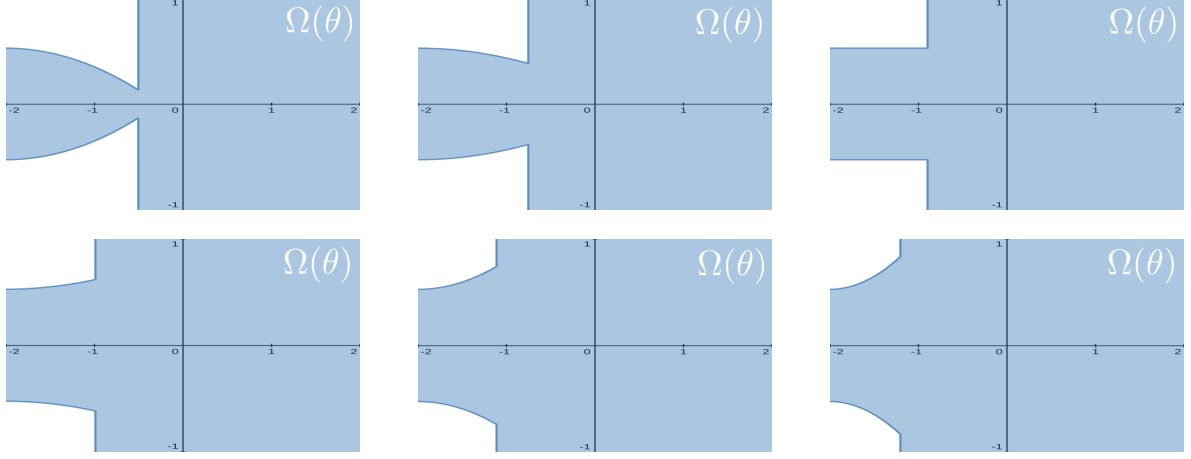


FIGURE 1. Six examples of solid walls, described by the levelset $\{\Phi_\theta = 0\}$. From left to the right, the levelset for $\theta = -0.1, -0.06, 0, 0.18, 0.37, 0.50$.

intersected by the physical domain:

$$\begin{aligned}\mathcal{I}_h &:= \{T \in \hat{\mathcal{I}}_h : \Omega \cap T \neq \emptyset\}, \\ \mathcal{F}_h &:= \{F \in \mathcal{F} : F \text{ is a facet of an element } T \in \mathcal{I}_h\}.\end{aligned}$$

Then, starting from the active mesh we can define a domain Ω_h^* as follows:

$$\Omega_h^* = \bigcup_{T \in \mathcal{I}_h} T.$$

We clarify that \mathcal{I}_h is a

- *boundary fitted mesh* if $\overline{\Omega_h^*} = \overline{\Omega}$;
- *unfitted mesh* if $\overline{\Omega} \subsetneq \overline{\Omega_h^*}$. In this case Ω_h^* is the so called *fictitious domain*.

For unfitted meshes an important role is played by the part of Γ intersecting elements T , $\Gamma_T := \Gamma \cap T$, and by those elements of the active mesh that intersect the boundary Γ of the physical domain Ω :

$$\mathcal{I}_\Gamma := \{T \in \mathcal{I}_h : T \cap \Gamma \neq \emptyset\}.$$

Related to the set \mathcal{I}_Γ we can also define the set of facets that belong to elements intersected by the boundary:

$$\mathcal{F}_\Gamma := \{F \in \mathcal{F} : F \text{ is a facet of an element } T \in \mathcal{I}_\Gamma\};$$

this set will become important in the next paragraph, when we introduce the Ghost Penalty (GP) stabilization. Finally we define the approximation space

$$\mathcal{H}_h := \{v_h \in C_0(\Omega_h^*) : v_h|_T \in \mathcal{P}^k(T), \quad \forall T \in \mathcal{I}_h\},$$

which is the space of continuous functions over Ω_h^* , which are polynomials of degree k on each element of the active mesh.

2.2. Steady Navier–Stokes. In the following, we focus on the steady incompressible Navier–Stokes equations, which are formulated within an Eulerian formalism. We first introduce the problem formulation, and then we present the discretized version of the original problem, in the CutFEM framework.

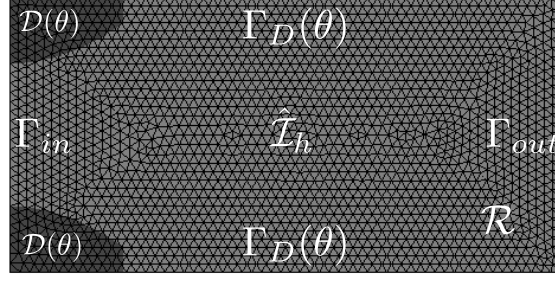


FIGURE 2. Mesh and geometry of the problem: the fluid domain (light grey) has an inlet boundary Γ_{in} on the left and an outlet boundary Γ_{out} on the right. The rest of the boundaries (Γ_D) are Dirichlet type boundaries. The solid domain is depicted in dark grey. Its shape is described through a levelset function and varies according to a parameter θ . This instance corresponds to $\theta = 0.37$.

TABLE 1. Values for the constants in the levelset equation (2).

Constant	Value
k_1	10
k_2	10
k_3	-2
k_4	-1
k_5	1

2.2.1. *Strong formulation.* Let \mathcal{R} be a background rectangular domain in \mathbb{R}^2 , and let $\mathcal{D}(\theta) \subset \mathcal{R}$ be a bounded subset of \mathcal{R} , whose boundary is described through a levelset function $\{\Phi_\theta = 0\}$, where Φ_θ is an implicit function depending on a geometrical parameter θ . The physical domain over which our problem is formulated is $\Omega(\theta) := \mathcal{R} \setminus \mathcal{D}(\theta)$. We denote by \mathcal{P} the parameter space to which θ belongs. Under these assumptions, our problem of interest reads: for every $\theta \in \mathcal{P}$, find $\mathbf{u}(\theta): \Omega(\theta) \mapsto \mathbb{R}^2$ and $p(\theta): \Omega(\theta) \mapsto \mathbb{R}$ such that:

$$(1) \quad \begin{cases} -\nu \Delta \mathbf{u}(\theta) + \nabla p(\theta) + (\mathbf{u}(\theta) \cdot \nabla) \mathbf{u}(\theta) = \mathbf{f}(\theta) & \text{in } \Omega(\theta), \\ \operatorname{div} \mathbf{u}(\theta) = 0 & \text{in } \Omega(\theta), \\ \mathbf{u}(\theta) = \mathbf{u}_{in}(\theta) & \text{on } \Gamma_{in}(\theta), \end{cases}$$

where ν is the fluid kinematic viscosity, $\mathbf{f}(\theta)$ is the fluid volume external force, and $\mathbf{u}_{in}(\theta)$ is a prescribed inlet velocity.

2.2.2. *Geometrical parametrization.* Figure 2 shows the background domain \mathcal{R} (light and dark grey), with the background mesh $\hat{\mathcal{I}}_h$, the physical domain $\Omega(\theta)$ (light grey) and the domain $\mathcal{D}(\theta)$ (dark grey). For the problem considered in this section the expression of the levelset function is the following:

$$(2) \quad \begin{aligned} \Phi_\theta(x, y) = & - \left(|A(x) + B(x) - 1| + |A(x) - B(x) - 2| + D(x) \right) \\ & \cdot \left(|A(x) + C(x) - 1| + |A(x) - C(x) - 2| + D(x) \right), \end{aligned}$$

where $A(x) = \sqrt{k_1} |x - k_3|$, $B(x) = \sqrt{k_2} |y - k_4|$, $C(x) = \sqrt{k_2} |y - k_5|$ and $D(x) = e^{-\theta} (k_1 (x - k_3)^2) \theta - 4$. The values of the constants k_1, k_2, k_3, k_4, k_5 are reported in Table 1. To have a better idea of how the shape of the walls changes by varying the parameter θ , the reader is referred to Figure 1.

2.2.3. *Discrete weak formulation and algebraic formulation.* As we can see from Figure 2, the background mesh $\hat{\mathcal{T}}_h$ is a rectangular mesh made by triangular elements. By choosing an unfitted mesh, once we have defined a background mesh, there is no need to remesh every time the parameter θ varies and hence every time the shape of the levelset (dark grey in Figure 2) changes.

In order to state a proper discretized weak formulation of the problem in this unfitted framework, we need some stabilization terms in the discretized weak formulation, in order to control polynomials on the cut elements. Let us introduce the following discrete approximation spaces:

$$\begin{aligned} V_{h,k}(\theta) &:= \{\mathbf{v}_h \in C_0(\Omega_h^*(\theta))^2: \mathbf{v}_h|_T \in (\mathcal{P}^k(T))^2, \quad \forall T \in \mathcal{I}_h(\theta)\}, \\ Q_{h,1}(\theta) &:= \{q_h \in C_0(\Omega_h^*(\theta)): q_h|_T \in \mathcal{P}^1(T), \quad \forall T \in \mathcal{I}_h(\theta)\}, \end{aligned}$$

where $\mathcal{I}_h(\theta)$ and $\Omega_h^*(\theta)$ are the active mesh and the fictitious domain respectively, as defined in Section 2.1. We remark that these spaces depend on θ , since the levelset geometry changes according to the parameter θ . The discretized weak formulation of the problem, with Nitsche's Method and Ghost Penalty terms then reads: find $(\mathbf{u}_h(\theta), p_h(\theta)) \in V_{h,1}(\theta) \times Q_{h,1}(\theta)$ such that for all test functions $(\mathbf{v}_h(\theta), q_h(\theta)) \in V_{h,1}(\theta) \times Q_{h,1}(\theta)$:

$$(3) \quad \mathcal{A}(\mathbf{u}_h(\theta), p_h(\theta), \mathbf{v}_h(\theta), q_h(\theta)) = \mathcal{L}(\mathbf{v}_h(\theta)),$$

where:

$$\begin{aligned} \mathcal{A}(\mathbf{u}_h(\theta), p_h(\theta), \mathbf{v}_h(\theta), q_h(\theta)) &= a(\mathbf{u}_h(\theta), \mathbf{v}_h(\theta); \theta) + d(\mathbf{u}_h(\theta), \mathbf{u}_h(\theta), \mathbf{v}_h(\theta); \theta) \\ &\quad - b(p_h(\theta), \mathbf{v}_h(\theta); \theta) + b(q_h(\theta), \mathbf{u}_h(\theta); \theta) \\ &\quad - \hat{b}(q_h(\theta), \mathbf{u}_h(\theta); \theta) + j_{\text{NIT}}(\mathbf{u}_h(\theta), \mathbf{v}_h(\theta); \theta) \\ &\quad + j_{\text{IP/GP}}^u(\mathbf{u}_h(\theta), \mathbf{v}_h(\theta); \theta) - j_{\text{IP/GP}}^p(p_h(\theta), q_h(\theta); \theta), \\ \mathcal{L}(\mathbf{v}_h) &= \int_{\Omega_h^*(\theta)} f(\theta) \mathbf{v}_h(\theta). \end{aligned}$$

More precisely we have the following terms:

$$\begin{aligned} a(\mathbf{u}_h(\theta), \mathbf{v}_h(\theta); \theta) &= \int_{\Omega_h^*(\theta)} \nu \nabla \mathbf{u}_h(\theta) : \nabla \mathbf{v}_h(\theta) - \sum_{T \in \mathcal{I}_T(\theta)} \int_{\Gamma_T} \nu \partial_n \mathbf{u}_h(\theta) \cdot \mathbf{v}_h(\theta) \\ &\quad - \sum_{T \in \mathcal{I}_T(\theta)} \int_{\Gamma_T} \nu \partial_n \mathbf{v}_h(\theta) \cdot \mathbf{u}_h(\theta), \\ d(\mathbf{u}_h(\theta), \mathbf{u}_h(\theta), \mathbf{v}_h(\theta); \theta) &= \int_{\Omega_h^*(\theta)} ((\mathbf{u}_h(\theta) \cdot \nabla) \mathbf{u}_h(\theta)) \cdot \mathbf{v}_h(\theta), \\ b(p_h(\theta), \mathbf{v}_h(\theta); \theta) &= \int_{\Omega_h^*(\theta)} p_h(\theta) \text{div} \mathbf{v}_h(\theta), \\ \hat{b}(q_h(\theta), \mathbf{u}_h(\theta); \theta) &= \sum_{T \in \mathcal{I}_T(\theta)} \int_{\Gamma_T} q_h(\theta) \mathbf{n} \cdot \mathbf{u}_h(\theta), \\ j_{\text{NIT}}(\mathbf{u}_h(\theta), \mathbf{v}_h(\theta); \theta) &= \nu \frac{\gamma_1}{h} \sum_{T \in \mathcal{I}_T(\theta)} \int_{\Gamma_T} \mathbf{u}_h(\theta) \mathbf{v}_h(\theta) + \frac{\gamma_2}{h} \sum_{T \in \mathcal{I}_T(\theta)} \int_{\Gamma_T} (\mathbf{u}_h(\theta) \cdot \mathbf{n})(\mathbf{v}_h(\theta) \cdot \mathbf{n}), \end{aligned}$$

TABLE 2. Constants values for the weak formulation of the problem

Constant	Value	Constant	Value
ν	0.05	h	0.07
γ_1	10	γ_2	10
α	0.1	g_u	0.001
γ_p	0.1	γ_g	0.1
λ_s	10	γ_s	(0.1, 0.01)

$$\begin{aligned}
j_{\text{IP/GP}}^u(\mathbf{u}_h(\theta), \mathbf{v}_h(\theta); \theta) &= \sum_{F \in \mathcal{F}_h(\theta)} \alpha \nu h^2 \|\mathbf{u}_h(\theta)\|_{\infty, T} \int_F \llbracket \text{div}(\mathbf{u}_h)(\theta) \rrbracket \llbracket \text{div}(\mathbf{v}_h)(\theta) \rrbracket \\
&+ \sum_{F \in \mathcal{F}_h(\theta)} g_u \nu h^2 \|\mathbf{u}_h \cdot \mathbf{n}_F\|_{\infty, F} \int_F \llbracket \partial_n(\mathbf{u}_h)(\theta) \rrbracket \llbracket \partial_n(\mathbf{v}_h)(\theta) \rrbracket \\
&+ \sum_{F \in \mathcal{F}_T(\theta)} \gamma_u \nu h \int_F \llbracket \partial_n(\mathbf{u}_h)(\theta) \rrbracket \llbracket \partial_n(\mathbf{v}_h)(\theta) \rrbracket, \\
j_{\text{IP/GP}}^p(p_h(\theta), q_h(\theta); \theta) &= \sum_{F \in \mathcal{F}_h(\theta)} \frac{\gamma_p h^3}{\nu} \frac{1}{\max(\frac{h}{\nu} \|\mathbf{u}(\theta)\|_{\infty, T}, 1)} \int_F \llbracket \partial_n p_h(\theta) \rrbracket \llbracket \partial_n q_h(\theta) \rrbracket.
\end{aligned}$$

The terms $a(\mathbf{u}_h(\theta), \mathbf{v}_h(\theta); \theta)$, $b(p_h(\theta), \mathbf{v}_h(\theta); \theta)$, $d(\mathbf{u}_h(\theta), \mathbf{u}_h(\theta), \mathbf{v}_h(\theta); \theta)$, and $\hat{b}(q_h(\theta), \mathbf{u}_h(\theta); \theta)$ come from the weak formulation of the incompressible Navier–Stokes equation, with Nitsche terms to impose the Dirichlet boundary condition. The expressions $j_{\text{NIT}}(\mathbf{u}_h(\theta), \mathbf{v}_h(\theta); \theta)$, correspond to Nitsche Penalties. The Interior and Ghost Penalty terms $j_{\text{IP/GP}}^u(\mathbf{u}_h(\theta), \mathbf{v}_h(\theta); \theta)$ and $j_{\text{IP/GP}}^p(p_h(\theta), q_h(\theta); \theta)$ contain stabilization terms that are necessary whenever the discretization spaces do not satisfy the inf–sup condition (e.g. for \mathbf{u}_h/p_h equal order spaces), stability in the extended area as well as the embedded boundary data weak enforcement. The values of the constants appearing in the previous equations are reported in Table 2. As we can see from the previous definitions, $\mathbf{u}_h(\theta)$ belongs to a space that is θ –dependent, namely $V_{h,1}(\theta)$, and the same goes for the pressure $p_h(\theta) \in Q_{h,1}(\theta)$. In order to define solutions on the whole background mesh, we employ a *natural smooth extension* of both velocity and pressure. In this way we obtain snapshots $(\hat{\mathbf{u}}_h(\theta), \hat{p}_h(\theta))$ that are defined on the common background mesh $\hat{\mathcal{T}}_h$; the reader interested in a detailed discussion on the natural smooth extension and on alternative techniques to extend the snapshots to the background mesh is referred to [4]. Such extension defines a pair of velocity–pressure snapshots $(\hat{\mathbf{u}}_h(\theta), \hat{p}_h(\theta))$ belonging to θ –independent discrete spaces:

$$\begin{aligned}
\hat{V}_{h,k} &:= \{\hat{\mathbf{v}}_h \in C_0(\mathcal{R})^2 : \hat{\mathbf{v}}_h|_T \in (\mathcal{P}^k(T))^2, \quad \forall T \in \hat{\mathcal{T}}_h\}, \\
\hat{Q}_{h,1} &:= \{\hat{q}_h \in C_0(\mathcal{R}) : \hat{q}_h|_T \in \mathcal{P}^1(T), \quad \forall T \in \hat{\mathcal{T}}_h\}.
\end{aligned}$$

In order to state the algebraic formulation equivalent to (3), let us introduce the following bijection between $\hat{V}_{h,1}$ and $\mathbb{R}^{N_u^h}$ (respectively $\hat{Q}_{h,1}$ and $\mathbb{R}^{N_p^h}$), where N_u^h and N_p^h are the dimensions of the discrete spaces $\hat{V}_{h,1}$ and $\hat{Q}_{h,1}$:

$$(4) \quad \begin{cases} \hat{\mathbf{v}}_h = (\hat{v}_h^1, \dots, \hat{v}_h^{N_u^h})^T \in \mathbb{R}^{N_u^h} & \iff \hat{\mathbf{v}}_h = \sum_{i=1}^{N_u^h} \hat{v}_h^i \boldsymbol{\varphi}^i \in \hat{V}_{h,1}, \\ \hat{q}_h = (\hat{q}_h^1, \dots, \hat{q}_h^{N_p^h})^T \in \mathbb{R}^{N_p^h} & \iff \hat{q}_h = \sum_{i=1}^{N_p^h} \hat{q}_h^i \zeta^i \in \hat{Q}_{h,1}, \end{cases}$$

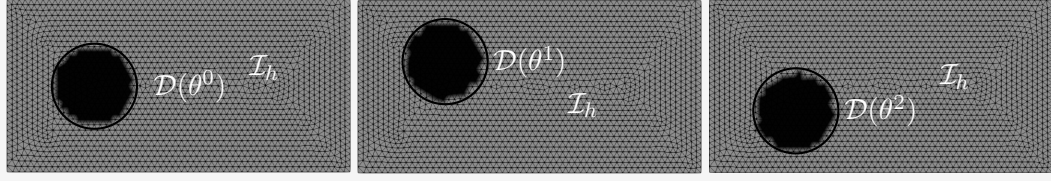


FIGURE 3. Time-dependent levelset: The physical domain at different times t_0, t_1, t_2 . The circular line represents the cylinder $\mathcal{D}(\theta)$ immersed in the fluid: the cylinder is moving up and down, so that the levelset function defining $\mathcal{D}(\theta)$ is time dependent. \mathcal{I}_h corresponds to the active mesh (light grey mesh) and it is related to the discretization of the unfitted/extended geometry.

where φ^i and ζ^i are the *parameter-independent* basis functions of the FE spaces $\hat{V}_{h,1}$ and $\hat{Q}_{h,1}$ respectively. Thanks to this bijection we can define the following matrices:

$$\begin{aligned} \mathbf{A}(\theta)_{ij} &:= a(\varphi^i, \varphi^j, \theta) + j_{\text{NIT}}(\varphi^i, \varphi^j, \theta) + j_{\text{IP/GP}}^u(\varphi^i, \varphi^j, \theta), \\ \mathbf{N}(\hat{\mathbf{u}}_h(\theta); \theta)_{ij} &:= \sum_{k=1}^{N_u^h} \hat{u}_h^k(\theta) d(\varphi^k, \varphi^i, \varphi^j; \theta), \\ \mathbf{B}(\theta)_{ij} &:= -b(\zeta^i, \varphi^j, \theta), \\ \hat{\mathbf{B}}(\theta)_{ij} &:= \hat{b}(\zeta^i, \varphi^j, \theta), \\ \mathbf{C}(\theta)_{ij} &:= j_{\text{IP/GP}}^p(\zeta^i, \zeta^j; \theta). \end{aligned}$$

Thanks to the introduced notation, we can conclude that equation (3) is equivalent to the following algebraic system:

$$R(\hat{U}_h(\theta), \theta) := \begin{bmatrix} \mathbf{A}(\theta) + \mathbf{N}(\hat{\mathbf{u}}_h(\theta); \theta) & \mathbf{B}^T(\theta) \\ \mathbf{B}(\theta) + \hat{\mathbf{B}}(\theta) & \mathbf{C}(\theta) \end{bmatrix} \begin{bmatrix} \hat{\mathbf{u}}_h(\theta) \\ \hat{\mathbf{p}}_h(\theta) \end{bmatrix} - \begin{bmatrix} \mathbf{F}_1(\theta) \\ \mathbf{F}_2(\theta) \end{bmatrix} = \begin{bmatrix} 0 \\ 0 \end{bmatrix},$$

where $\hat{U}_h(\theta) = (\hat{\mathbf{u}}_h(\theta), \hat{\mathbf{p}}_h(\theta))$, $(\mathbf{F}_1(\theta))_i := \int_{\Omega_h^*(\theta)} \varphi^i \cdot \mathbf{f} \, dx$, and $\mathbf{F}_2(\theta) = \mathbf{0}$.

We point out that the aforementioned formulation, defined on the whole background mesh, is actually required only by the ROM procedure. The CutFEM formulation is defined only on the active mesh \mathcal{I}_h and the extended geometry Ω_h^* .

2.3. Unsteady Navier–Stokes. We now extend the previous treatment to the unsteady incompressible Navier–Stokes problem, by introducing the time evolution term $\partial_t \mathbf{u}(\theta)$ in system (1).

2.3.1. Strong formulation. Given a time interval of interest $[0, T]$, the strong formulation of the problem reads as follows: for every $\theta \in \mathcal{P}$, and for every $t \in [0, T]$, find $\mathbf{u}(t; \theta): \Omega(\theta) \mapsto \mathbb{R}^2$ and $p(t; \theta): \Omega(\theta) \mapsto \mathbb{R}$ such that:

$$(5) \quad \begin{cases} \partial_t \mathbf{u}(\theta) - \nu \Delta \mathbf{u}(\theta) + \nabla p(\theta) + (\mathbf{u}(\theta) \cdot \nabla) \mathbf{u}(\theta) = \mathbf{f}(\theta) & \text{in } \Omega(\theta) \times [0, T], \\ \operatorname{div} \mathbf{u}(\theta) = 0 & \text{in } \Omega(\theta) \times [0, T], \\ \mathbf{u}(\theta) = \mathbf{u}_{in} & \text{on } \Gamma_{in}(\theta) \times [0, T], \\ \mathbf{u}(\mathbf{x}, 0; \theta) = \mathbf{u}^0(\mathbf{x}, \theta) & \text{in } \Omega(\theta), \end{cases}$$

with geometrical parameterization identical to that in the previous subsection. We remark that here the geometrical parametrization does not evolve in time, i.e. $\frac{d\theta}{dt} = 0$. We will consider the case of $\frac{d\theta}{dt} \neq 0$ in the next Section 2.4.

2.3.2. Space discretization, time-stepping scheme and algebraic formulation. We discretize in time by an implicit-explicit Euler approach, see e.g. [33]. We discretize the time interval $[0, T]$ with the following partition:

$$0 = t^0 < \dots < t^{N_t} = T,$$

where every interval $(t^n, t^{n+1}]$ has measure $\tau_{n+1} = t^{n+1} - t^n$, $n = 0, \dots, N_t - 1$. The discrete version of the initial condition $\mathbf{u}^0(x; \theta)$ is denoted by $\mathbf{u}_h^0(x; \theta)$; we denote \mathbf{u}_h^n the discrete fluid velocity at time step t^n , and similar notation is used for the pressure. After having applied a time stepping scheme, the space discretized weak formulation of the problem reads as follows: for every $n = 0, \dots, N_t - 1$, we seek a discrete velocity $\mathbf{u}_h^{n+1}(\theta) \in V_{h,2}(\theta)$ and discrete pressure $p_h^{n+1}(\theta) \in Q_{h,1}(\theta)$, such that for every $(\mathbf{v}_h(\theta), q_h(\theta)) \in V_{h,2}(\theta) \times Q_{h,1}(\theta)$, it holds:

$$m(\mathbf{u}_h^{n+1}(\theta) - \mathbf{u}_h^n(\theta), \mathbf{v}_h) + \tau_{n+1} \mathcal{A}(\mathbf{u}_h^{n+1}(\theta), p_h^{n+1}(\theta), \mathbf{v}_h(\theta), q_h(\theta)) = \tau_{n+1} \mathcal{L}(\mathbf{v}_h(\theta)),$$

where

$$m(\mathbf{w}_h, \mathbf{v}_h) := \int_{\Omega_h^*(\theta)} \mathbf{w}_h \cdot \mathbf{v}_h \, dx,$$

and where $\mathcal{A}(\mathbf{u}_h^{n+1}(\theta), p_h^{n+1}(\theta), \mathbf{v}_h(\theta), q_h(\theta))$ and $\mathcal{L}(\mathbf{v}_h(\theta))$ are defined as in Section 2.2.3.

We employ again a natural smooth extension, as stated in the previous subsection. Keeping the notation previously introduced, and using the bijection (4), we introduce the *mass matrix* $\mathbf{M}_{ij} := m(\boldsymbol{\varphi}^i, \boldsymbol{\varphi}^j)$. Let now $\hat{\mathbf{U}}_h^{n+1}(\theta)$ be defined as $\hat{\mathbf{U}}_h^{n+1}(\theta) := (\hat{\mathbf{u}}_h^{n+1}, \hat{p}_h^{n+1})$; using the notation introduced for the steady problem, the resulting fully-discrete time dependent cut Finite Element Navier-Stokes algebraic equation is

$$\begin{bmatrix} \mathbf{M} & \mathbf{0} \\ \mathbf{0} & \mathbf{0} \end{bmatrix} \hat{\mathbf{U}}_h^{n+1}(\theta) + \tau_{n+1} \mathbf{R}(\hat{\mathbf{U}}_h^{n+1}(\theta); \theta) = \begin{bmatrix} \mathbf{M} & \mathbf{0} \\ \mathbf{0} & \mathbf{0} \end{bmatrix} \hat{\mathbf{U}}_h^n(\theta).$$

2.4. Unsteady Navier-Stokes with time dependent geometry. We extend here the previous unsteady formulation to the case where the parameter θ is *time dependent*, i.e. $\partial_t \theta \neq 0$. For this test case we assume that $\mathcal{D}(\theta)$ represents a cylinder immersed in the fluid domain, and therefore we denote herein $\Gamma_{cyl}(\theta) = \partial \mathcal{D}(\theta)$.

2.4.1. Strong formulation. The problem reads as follows: for every $t \in [0, T]$ and for every $\theta(t) \in \mathcal{P}$, find $\mathbf{u}(t; \theta(t)) : \Omega(\theta(t)) \mapsto \mathbb{R}^2$, $p(t; \theta(t)) : \Omega(\theta(t)) \mapsto \mathbb{R}$ such that:

$$(6) \quad \begin{cases} \partial_t \mathbf{u}(\theta(t)) - \nu \Delta \mathbf{u}(\theta(t)) + \nabla p(\theta(t)) + (\mathbf{u}(\theta(t)) \cdot \nabla) \mathbf{u}(\theta(t)) = \mathbf{f}(\theta(t)) & \text{in } \Omega(\theta(t)) \times [0, T], \\ \operatorname{div} \mathbf{u}(\theta(t)) = 0 & \text{in } \Omega(\theta(t)) \times [0, T], \\ \mathbf{u}(\theta(t)) = \mathbf{u}_{in} & \text{on } \Gamma_{in}(\theta(t)) \times [0, T], \\ \mathbf{u}(\theta(t)) = \partial_t \theta & \text{on } \Gamma_{cyl}(\theta(t)) \times [0, T], \\ \mathbf{u}(\mathbf{x}, 0; \theta(t)) = \mathbf{u}^0(\mathbf{x}, \theta(t)) & \text{in } \Omega(\theta(t)), \end{cases}$$

where $\partial_t \theta$ denotes the velocity with which the cylinder $\mathcal{D}(\theta(t))$ moves in the domain.

2.4.2. Geometrical parametrization. The obstacle immersed in the fluid domain in our problem is a parametrized circle, defined through the *time dependent* levelset function:

$$\phi(x, y, \theta_1(t), \theta_2(t)) = (x - \theta_1(t))^2 + (y - \theta_2(t))^2 - R^2,$$

where $\theta(t) = (\theta_1(t), \theta_2(t))$ denotes the position of the center of the cylinder in the domain, and R is the radius of the circle.

As we can see from the strong formulation of the problem, the motion of the cylinder is assumed to be known, i.e. it is not an unknown of the system, as it would be instead for a fully coupled fluid-structure interaction problem. For our simulations, we assume the motion of the cylinder to be periodic, i.e.

$$(7) \quad \theta(t) = \theta(0) + \operatorname{Asin}(8\pi\mu(t)) \underline{\mathbf{j}},$$

where A denotes the amplitude of the oscillation of the cylinder, $\mu(t)$ is a function of time and \underline{j} is a versor in the vertical direction; thus, the cylinder moves only vertically in our simulations. With this assumption, we can explicitly write the velocity of the cylinder $\partial_t \theta$, in fact:

$$\partial_t \theta(t) = A \frac{d\mu(t)}{dt} 8\pi \cos(\mu(t)8\pi) \underline{j}.$$

The Figure 3 shows the physical domain $\Omega(\theta)$ at different times t_0, t_1, t_2 , for the time dependent levelset function $\theta(t)$ defining $\mathcal{D}(\theta)$.

2.4.3. Weak formulation and time discretization. We now want to state the weak formulation of the original problem after discretization in space and after having applied a time stepping scheme. As far as the time discretization concerns, we employ the time stepping scheme adopted in the previous subsection for the unsteady Navier-Stokes problem: we discretize the time interval $[0, T]$ in sub-intervals $(t^n, t^{n+1}]$ of measure $\tau_{n+1} = t^{n+1} - t^n$, for $n = 0, \dots, N_t - 1$. Let us denote with $\theta^n = \theta(t^n)$ the value of the geometrical parameter at time t^n .

For the space discretization, let us introduce the following discrete spaces at time-step t^{n+1} :

$$\begin{aligned} V_{h,2}(\theta^{n+1}) &:= \{\mathbf{v}_h \in (C_0(\Omega_h^*(\theta^{n+1})))^2 : \mathbf{v}_h|_T \in (\mathcal{P}^2(T))^2, \quad \forall T \in \mathcal{I}_h(\theta^{n+1})\}, \\ Q_{h,1}(\theta^{n+1}) &:= \{q_h \in C_0(\Omega_h^*(\theta^{n+1})) : q_h|_T \in \mathcal{P}^1(T), \quad \forall T \in \mathcal{I}_h(\theta^{n+1})\}. \end{aligned}$$

As we can see from the previous definitions, the discrete spaces $V_{h,2}(\theta^{n+1})$ and $Q_{h,1}(\theta^{n+1})$ depend now not only on the geometrical parameter θ , but also on time t ; in fact, even though the background mesh $\hat{\mathcal{I}}_h$ remains fixed, the active mesh \mathcal{I}_h , the fictitious domain Ω_h^* , the cut elements in \mathcal{I}_Γ and other relevant entities, change in time according to the change of the levelset function. After applying a time stepping scheme, the weak formulation of the original problem reads: at timestep t^{n+1} , find $(\mathbf{u}_h^{n+1}(\theta^{n+1}), p_h^{n+1}(\theta^{n+1})) \in V_{h,2}(\theta^{n+1}) \times Q_{h,1}(\theta^{n+1})$ such that, for all $(\mathbf{v}_h, q_h) \in V_{h,2}(\theta^{n+1}) \times Q_{h,1}(\theta^{n+1})$:

$$\begin{aligned} (8) \quad & m(\mathbf{u}_h^{n+1}(\theta^{n+1}) - \mathbf{u}_h^n(\theta^n), \mathbf{v}_h(\theta^{n+1})) + \tau_{n+1} \mathcal{A}(\mathbf{u}_h^{n+1}(\theta^{n+1}), p_h^{n+1}(\theta^{n+1}), \mathbf{v}_h(\theta^{n+1}), q_h(\theta^{n+1})) = \\ & = \tau_{n+1} \mathcal{L}(\mathbf{v}_h(\theta^{n+1})), \end{aligned}$$

where we have kept the same notation as in the previous subsection. The problem now is that all the integrals appearing in equation (8) are evaluated over the fictitious domain at time-step t^{n+1} , namely $\Omega_h^*(\theta^{n+1})$: in general $\Omega_h^*(\theta^{n+1}) \neq \Omega_h^*(\theta^n)$, and thus $V_h^{n+1}(\theta^{n+1}) \neq V_h^n(\theta^n)$, so in general $\mathbf{u}_h^n(\theta^n) \notin V_h(\theta^{n+1})$. To overcome this problem we employ again a *natural smooth extension* of the snapshots $(\mathbf{u}_h^{n+1}(\theta^{n+1}), p_h^{n+1}(\theta^{n+1}))$, as already introduced in Section 2.2.3. We therefore recall the definition of the global discrete spaces defined on the background domain \mathcal{R} :

$$\begin{aligned} \hat{V}_{h,2} &:= \{\hat{\mathbf{v}}_h \in C_0(\mathcal{R})^2 : \hat{\mathbf{v}}_h|_T \in (\mathcal{P}^2(T))^2, \quad \forall T \in \hat{\mathcal{I}}_h\}, \\ \hat{Q}_{h,1} &:= \{\hat{q}_h \in C_0(\mathcal{R}) : \hat{q}_h|_T \in \mathcal{P}^1(T), \quad \forall T \in \hat{\mathcal{I}}_h\}, \end{aligned}$$

and, keeping the same notation previously introduced, we can recover the algebraic formulation of the problem, which reads: for every $n = 0, \dots, N_t - 1$, find $\hat{U}_h^{n+1}(\theta^{n+1}) := (\hat{\mathbf{u}}_h^{n+1}(\theta^{n+1}), \hat{p}_h^{n+1}(\theta^{n+1}))$ such that:

$$\begin{bmatrix} \mathbf{M} & \mathbf{0} \\ \mathbf{0} & \mathbf{0} \end{bmatrix} \hat{U}_h^{n+1}(\theta^{n+1}) + \tau_{n+1} R(\hat{U}_h^{n+1}(\theta^{n+1}); \theta) = \begin{bmatrix} \mathbf{M} & \mathbf{0} \\ \mathbf{0} & \mathbf{0} \end{bmatrix} \hat{U}_h^n(\theta^n).$$

3. PROPER ORTHOGONAL DECOMPOSITION-GALERKIN MODEL REDUCTION

In the present work, the Proper Orthogonal Decomposition (POD) method is applied to parameter-dependent matrices which have been derived from solution instances. The POD method consists of two phases: one *offline* and one *online*. During the offline phase, we compute the solution of the problem of interest, for different values of the parameters. These

parameters are collected from a training set \mathcal{P}_{train} , and the corresponding solutions are stored into a matrix, the so-called snapshots matrix. This matrix is then processed in order to extract the reduced basis. Afterwards, in the online phase, we employ these basis functions in a way that reduces the dimension of the original problem, and in a way that is computationally efficient for (in our case) geometrically parametrized systems.

We remind that for POD-Galerkin ROMs for incompressible Navier-Stokes equations, instabilities in the approximation of the pressure may occur. We refer to [12, 18, 35] for a more detailed analysis of the problem, while for such instabilities on transient problems we refer to [5, 10, 17, 24, 39]. For SUPG and PSPG kind of stabilization we refer to [7, 37, 41, 42]. Levelset techniques with cut Finite Element Nitsche method will be employed for the parametrization and ROM focusing on a fixed, geometrical parameter independent, background mesh following approaches as in [4, 27, 29].

3.1. Steady case. Next we denote by $\theta^{(j)}$ each parameter in a finite dimensional training set $\mathcal{P}_{train} = \{\theta^{(1)}, \dots, \theta^{(M)}\}$ for a large number M . We recall that the number of degrees of freedom considering the full order problem are denoted by N_u^h and N_p^h for the velocity and the pressure respectively. The collected snapshots matrices \mathcal{S}_u and \mathcal{S}_p , are then defined as follows:

$$(9) \quad \mathcal{S}_u = [\hat{\mathbf{u}}_h(\theta^{(1)}), \dots, \hat{\mathbf{u}}_h(\theta^{(M)})] \in \mathbb{R}^{N_u^h \times M}, \quad \mathcal{S}_p = [\hat{p}_h(\theta^{(1)}), \dots, \hat{p}_h(\theta^{(M)})] \in \mathbb{R}^{N_p^h \times M},$$

where $\hat{\mathbf{u}}_h$ and \hat{p}_h are vectors defined by the bijection (4).

In order to make the pressure approximation stable at the reduced order level we also introduce a velocity supremizer variable \mathbf{s}_h : see [7, 35, 37] for a more detailed introduction to the supremizer enrichment for Navier-Stokes equation. We start with a Poisson formulation for the supremizer $\mathbf{s}_h(\theta)$:

$$(\nabla \mathbf{s}_h(\theta), \nabla \mathbf{v}_h(\theta)) = -p_h(\theta) \operatorname{div} \mathbf{v}_h(\theta),$$

and by adding Nitsche terms and stabilization terms we obtain the following formulation:

$$\begin{aligned} (\nabla \mathbf{s}_h(\theta^{(i)}), \nabla \mathbf{v}_h(\theta^{(i)})) - (\nabla \mathbf{s}_h(\theta^{(i)}) \mathbf{n}, \mathbf{v}_h(\theta^{(i)})) - (\nabla \mathbf{v}_h(\theta^{(i)}) \mathbf{n}, \mathbf{s}_h(\theta^{(i)})) + \frac{\lambda_s}{h} (s_h(\theta^{(i)}), v_h(\theta^{(i)})) \\ + g^{GP}(\mathbf{s}_h(\theta^{(i)}), \mathbf{v}_h(\theta^{(i)})) = -p_h(\theta^{(i)}) \operatorname{div} \mathbf{v}_h(\theta^{(i)}), \end{aligned}$$

where the Ghost Penalty term is given by:

$$g^{GP}(\mathbf{s}_h(\theta^{(i)}), \mathbf{v}_h(\theta^{(i)})) = \sum_{0 \leq j \leq k} \gamma_s^j h^{2j+1} \langle \llbracket \partial_n^j \mathbf{s}_h(\theta^{(i)}) \rrbracket, \llbracket \partial_n^j \mathbf{v}_h(\theta^{(i)}) \rrbracket \rangle,$$

for all $j = 1, \dots, M$, where we recall that k is the degree of the piecewise polynomial FE basis functions on each element of the active mesh. The values of the constants used are reported in Table 2.

The formulation that we use for the supremizer enrichment is a special instance of a Poisson problem, and therefore, we use the CutFEM Poisson discretization for its approximation, component by component. We employ the same natural smooth extension (and the same extended FE space used for velocity) also for the supremizer, thus obtaining the extended snapshots $\hat{\mathbf{s}}_h$. These snapshots are then collected in the snapshot matrix

$$\mathcal{S}_s = [\hat{\mathbf{s}}_h(\theta^{(1)}), \dots, \hat{\mathbf{s}}_h(\theta^{(M)})] \in \mathbb{R}^{N_u^h \times M},$$

We then carry out a compression by POD on the snapshots matrices, namely \mathcal{S}_u , \mathcal{S}_s and \mathcal{S}_p , following e.g. [30]. This derives an eigenvalue problem, that for the velocity for example reads:

$$\mathcal{C}^u \mathbf{Q}^u = \mathbf{Q}^u \mathbf{\Lambda}^u, \quad \text{for } \mathcal{C}_{ij}^u = (\hat{\mathbf{u}}_h(\theta^{(i)}), \hat{\mathbf{u}}_h(\theta^{(j)}))_{L^2(\hat{\mathcal{T}}_h)}, \quad i, j = 1, \dots, M,$$

where \mathcal{C}^u is the correlation matrix derived from the θ -independent snapshots, \mathbf{Q}^u is an eigenvectors square matrix and $\mathbf{\Lambda}^u$ is a diagonal matrix of eigenvalues. Similar eigenvalue problems can be derived for the supremizer and for the pressure.

We then obtain a set $\{\boldsymbol{\Phi}_1^u, \dots, \boldsymbol{\Phi}_N^u, \boldsymbol{\Phi}_1^s, \dots, \boldsymbol{\Phi}_N^s\}$ of $2N$ basis functions for the reduced order

approximation of the velocity, and a set $\{\Phi_1^p, \dots, \Phi_N^p\}$ of N basis functions for the reduced order approximation of the pressure. We define: \hat{V}_N , the enriched reduced basis space for the velocity, and \hat{Q}_N , the reduced basis space for the pressure:

$$\hat{V}_N = \text{span}\{\Phi_1^{u,s}, \dots, \Phi_{2N}^{u,s}\}, \quad \hat{Q}_N = \text{span}\{\Phi_1^p, \dots, \Phi_N^p\}$$

where $N < M$ is chosen according to the eigenvalue decay of Λ_{ii}^u and Λ_{ii}^p , see for instance [9, 34]. We introduce the online velocity $\mathbf{u}_N(\theta)$ and the online pressure $p_N(\theta)$:

$$(10) \quad \mathbf{u}_N(\theta) := \sum_{i=1}^{2N} \underline{\mathbf{u}}_N^i(\theta) \Phi_i^{u,s} = \mathbf{L}_{u,s} \underline{\mathbf{u}}_N(\theta),$$

$$(11) \quad p_N(\theta) := \sum_{i=1}^N \underline{p}_N^i(\theta) \Phi_i^p = \mathbf{L}_p \underline{p}_N(\theta),$$

where $\mathbf{L}_{u,s}$ and \mathbf{L}_p are rectangular matrices containing the FE degrees of freedom of the basis of \hat{V}_N and \hat{Q}_N . The parameter *dependent* solution vector $\underline{\mathbf{u}}_N(\theta), \underline{p}_N(\theta) \in \mathbb{R}^N$ and the parameter *independent* reduced basis functions $\Phi_i^{u,s}, \Phi_i^p$ are the key ingredients necessary to perform a Galerkin projection of the full system onto the aforementioned reduced basis space. By introducing $U_N(\theta) = (\underline{\mathbf{u}}_N(\theta), \underline{p}_N(\theta))$, the formulation, at the reduced order level, of the steady Navier-Stokes problem, reads as follows:

$$\begin{bmatrix} \mathbf{L}_{u,s}^T (\mathbf{A}(\theta) + \mathbf{N}(\underline{\mathbf{u}}_N(\theta); \theta)) \mathbf{L}_{u,s} & \mathbf{L}_{u,s}^T \mathbf{B}^T(\theta) \mathbf{L}_p \\ \mathbf{L}_p^T (\mathbf{B}(\theta) + \hat{\mathbf{B}}(\theta)) \mathbf{L}_{u,s} & \mathbf{L}_p^T \mathbf{C}(\theta) \mathbf{L}_p \end{bmatrix} U_N(\theta) - \begin{bmatrix} \mathbf{L}_{u,s}^T \mathbf{F}_1(\theta) \\ \mathbf{L}_p^T \mathbf{F}_2(\theta) \end{bmatrix} = 0.$$

For the sake of the exposition, let us denote the vector on the left hand side of the above equation (the reduced residual) as $R_N(U_N(\theta); \theta)$. In the above POD-ROM solution, we clarify that we have to assemble the matrices of the high fidelity system. For a “cheaper” in time execution and less computation resources costs, one could achieve further improvement employing hyper reduction techniques as in [8, 13, 43, 45].

3.2. Unsteady case. Similarly to what has been done in the previous paragraph, in the time dependent case an *offline/online* procedure will be employed, that will lead to the generation of a proper reduced basis set. Since the system is both (geometrical) parameter and time-dependent, we sample not only the geometrical parameter θ , but also the time t , with the sample points $t^k \in \{t^0, \dots, t^{N_t}\} \subset [0, T]$. This procedure is computationally more expensive and results in a much larger total number of snapshots to be collected with respect to the static system: the total number of snapshots that we collect is now equal to $\widehat{M} = M \cdot N_t$. The snapshots matrices $\mathcal{S}_u, \mathcal{S}_s$ and \mathcal{S}_p are then given by:

$$(12) \quad \mathcal{S}_u = [\hat{\mathbf{u}}_h(\theta^{(1)}, t^0), \dots, \hat{\mathbf{u}}_h(\theta^{(1)}, t^{N_t}), \dots, \hat{\mathbf{u}}_h(\theta^{(M)}, t^0), \dots, \hat{\mathbf{u}}_h(\theta^{(M)}, t^{N_t})] \in \mathbb{R}^{N_u^h \times \widehat{M}},$$

$$(13) \quad \mathcal{S}_s = [\hat{\mathbf{s}}_h(\theta^{(1)}, t^0), \dots, \hat{\mathbf{s}}_h(\theta^{(1)}, t^{N_t}), \dots, \hat{\mathbf{s}}_h(\theta^{(M)}, t^0), \dots, \hat{\mathbf{s}}_h(\theta^{(M)}, t^{N_t})] \in \mathbb{R}^{N_s^h \times \widehat{M}},$$

$$(14) \quad \mathcal{S}_p = [\hat{\mathbf{p}}_h(\theta^{(1)}, t^0), \dots, \hat{\mathbf{p}}_h(\theta^{(1)}, t^{N_t}), \dots, \hat{\mathbf{p}}_h(\theta^{(M)}, t^0), \dots, \hat{\mathbf{p}}_h(\theta^{(M)}, t^{N_t})] \in \mathbb{R}^{N_p^h \times \widehat{M}},$$

and we solve an eigenvalue problem like the one introduced in the previous subsection. Finally, adopting the notation of subsection 3.1 we end up with the reduced basis spaces

$$\hat{V}_N = \text{span}\{\Phi_1^{u,s}, \dots, \Phi_{2N}^{u,s}\}, \quad \hat{Q}_N = \text{span}\{\Phi_1^p, \dots, \Phi_N^p\},$$

Let us now denote by $(\mathbf{u}_N^n(\theta), p_N^n(\theta))$ the reduced solution at time-step t^n , for $n = 0, \dots, N_t$, where $\mathbf{u}_N^n(\theta)$ and $p_N^n(\theta)$ are defined as in (10) and in (11), respectively. Through a Galerkin projection of the full-order system of equations onto the POD reduced basis spaces we can derive the subsequent reduced algebraic system for the unknown $U_h^{n+1}(\theta) = (\mathbf{u}_N^{n+1}(\theta), p_N^{n+1}(\theta))$:

$$(15) \quad \begin{bmatrix} \mathbf{L}_{u,s}^T \mathbf{M} \mathbf{L}_{u,s} & \mathbf{0} \\ \mathbf{0} & \mathbf{0} \end{bmatrix} U_N^{n+1}(\theta) + \tau_{n+1} R_N(U_N^{n+1}(\theta); \theta) = \begin{bmatrix} \mathbf{L}_{u,s}^T \mathbf{M} \mathbf{L}_{u,s} & \mathbf{0} \\ \mathbf{0} & \mathbf{0} \end{bmatrix} U_N^n(\theta).$$

3.3. Unsteady case with time-dependent geometry. For the unsteady Navier-Stokes with time-dependent geometry we sample the time interval $[0, T]$ with the sample points $\{t^0, \dots, t^{N_t}\}$; for each sample point t^n we then compute the corresponding geometrical parameter θ^n , for $n = 0, \dots, N_t$. Thus, in this case, the snapshots matrices \mathcal{S}_u , \mathcal{S}_s and \mathcal{S}_p are:

$$(16) \quad \mathcal{S}_u = [\underline{\mathbf{u}}_h(\theta^0, t^0), \dots, \underline{\mathbf{u}}_h(\theta^{N_t}, t^{N_t})] \in \mathbb{R}^{N_u^h \times N_t},$$

$$(17) \quad \mathcal{S}_s = [\underline{\mathbf{s}}_h(\theta^0, t^0), \dots, \underline{\mathbf{s}}_h(\theta^{N_t}, t^{N_t})] \in \mathbb{R}^{N_s^h \times N_t},$$

$$(18) \quad \mathcal{S}_p = [\underline{\mathbf{p}}_h(\theta^0, t^0), \dots, \underline{\mathbf{p}}_h(\theta^{N_t}, t^{N_t})] \in \mathbb{R}^{N_p^h \times N_t},$$

Again, by adopting the notation of subsection 3.1 we end up with the reduced basis spaces

$$\hat{V}_N = \text{span}\{\Phi_1^{u,s}, \dots, \Phi_{2N}^u\}, \quad \hat{Q}_N = \text{span}\{\Phi_1^p, \dots, \Phi_N^p\},$$

We denote by $(\mathbf{u}_N^n(\theta^n), p_N^n(\theta^n))$ the reduced solution at timestep t^n , for $n = 0, \dots, N_t$, defined as in (10) and (11). We employ again a Galerkin projection of the full-order system of equations onto the POD reduced basis spaces; we derive the subsequent reduced algebraic system of equations for the unknown $U_N^{n+1}(\theta) = (\mathbf{u}_N^n(\theta^n), p_N^n(\theta^n))$:

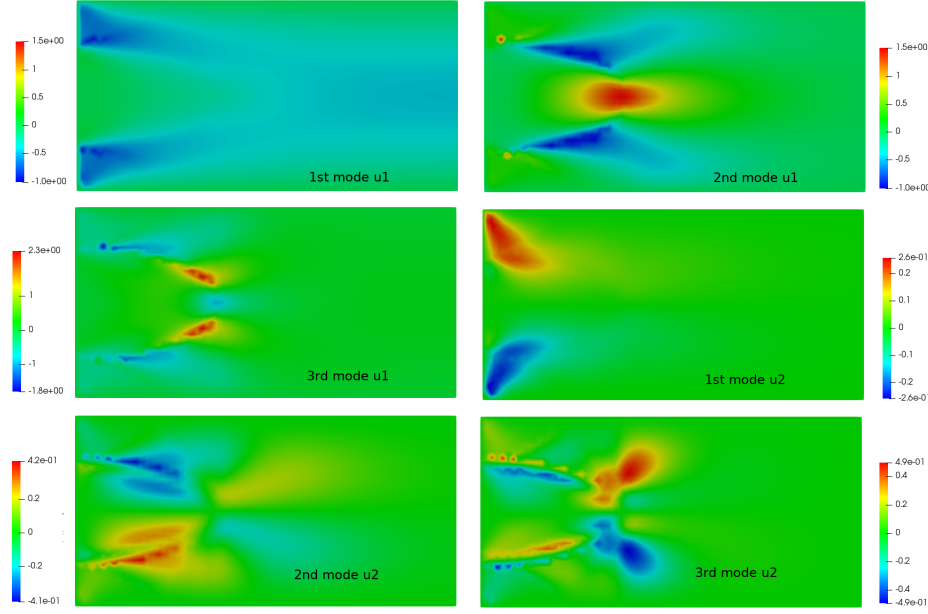
$$(19) \quad \begin{bmatrix} \mathbf{L}_{u,s}^T \mathbf{M} \mathbf{L}_{u,s} & \mathbf{0} \\ \mathbf{0} & \mathbf{0} \end{bmatrix} U_N^{n+1}(\theta^{n+1}) + \tau_{n+1} R_N(U_N^{n+1}(\theta^{n+1}); \theta^{n+1}) = \begin{bmatrix} \mathbf{L}_{u,s}^T \mathbf{M} \mathbf{L}_{u,s} & \mathbf{0} \\ \mathbf{0} & \mathbf{0} \end{bmatrix} U_N^n(\theta^n).$$

Remark 3.1. Here we have underlined the dependence of the geometrical parameter θ on time t because in the strong formulation of the original problem the geometry of the domain is time dependent; nevertheless we would like to recall that we chose to implement a natural smooth extension of the discrete CutFEM solution, therefore all the snapshots, as well as the reduced solution, are defined on the whole background mesh.

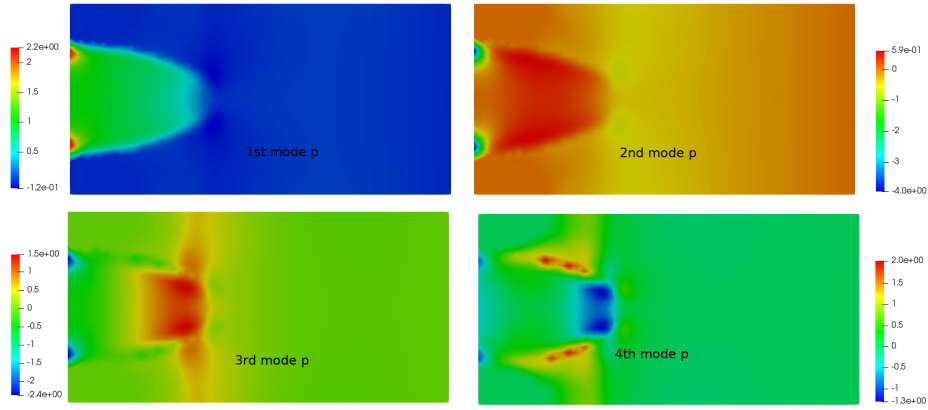
4. NUMERICAL RESULTS

4.1. Steady Navier-Stokes. In this paragraph we present the results obtained by applying the aforementioned reduction techniques to our model problem. For our simulation, the fluid viscosity is $\nu_f = 0.05 \text{ cm}^2/\text{s}$ and the fluid density is $\rho_f = 1 \text{ g/cm}^3$. We impose a constant velocity profile at the inlet, $\mathbf{u}_{\text{in}} = (1, 0)$, and we impose a homogeneous condition on the vertical component of the velocity at the top and bottom walls of the rectangle. The reduced basis have been obtained with a Proper Orthogonal Decomposition on the set of snapshots: this reduction technique, although costly in computational terms, is very useful as it gives an insight on the rate of decay of the eigenvalues related to each component of the solution. We take $N_{\text{train}} = 150$, and we generate randomly N_{train} uniformly distributed values for the parameter θ . We then run a POD on the collected set of snapshots and we obtain our basis functions, with which we are going to compute the reduced solutions $(\mathbf{u}_N(\theta^{(i)}), p_N(\theta^{(i)}))$, where $i = 1, \dots, N_{\text{test}}$, and N is the number of basis functions that we use. Figures 4(a) and 4(b) give an example of the first modes that we obtain with this procedure, whereas in Figure 5 we report the decay of the eigenvalues for all the components of the solution and for the supremizer. To test the reduced order model we generate randomly $N_{\text{test}} = 30$ uniformly distributed values values for $\theta \in \mathcal{P}_{\text{test}}$. We are interested in the behavior of the relative approximation error that we obtain by changing the number of basis functions N used to build the reduced solution. In order to do this we let N vary in a discrete set \mathcal{N} : for a fixed value of $N \in \mathcal{N}$, and for each $\theta^{(i)}$, $i = 1, \dots, N_{\text{test}}$, we compute both the reduced solution $(\mathbf{u}_N(\theta^{(i)}), p_N(\theta^{(i)}))$ and the corresponding full order solution $(\mathbf{u}_h(\theta^{(i)}), p_h(\theta^{(i)}))$. We compute the L^2 relative error $\epsilon_u^{N,i}$ for the velocity and the relative error $\epsilon_p^{N,i}$ for the pressure; then we compute the average approximation errors $\bar{\epsilon}_u^N$ and $\bar{\epsilon}_p^N$ for every $N \in \mathcal{N}$, defined as:

$$\bar{\epsilon}_u^N = \frac{1}{N_{\text{test}}} \sum_{i=1}^{N_{\text{test}}} \epsilon_u^{N,i}.$$



(a) First six modes for the velocity.



(b) First four modes for the pressure.

FIGURE 4. Steady system: Some reduced basis modes for velocity and pressure for a geometrically parametrized Navier-Stokes system.

Figure 6 shows the relative approximation errors plotted against the number N of basis functions used, with the use of the supremizer enrichment at the reduced order level and without the supremizer enrichment, respectively. As we can see, using a supremizer enrichment at the reduced level allows us to obtain a better approximation of the pressure: we have almost one order of magnitude of difference in the relative error with $N = 20$ basis functions for the pressure, with or without the supremizer. Figure 7(b) shows the approximation error for the pressure, for a given test value of the parameter θ , without the supremizer enrichment; the error has been calculated in the L^2 norm. Figure 7(a) shows the approximation error for the pressure, for the same parameter value, with the supremizer enrichment: as we can see, the supremizer is useful in obtaining a much more accurate approximation of the reduced order pressure. It is worth to mention that the approximation error tends to concentrate near the cut between the physical domain and the background mesh, similar to to experiments in the works of [4, 26–28], phenomenon which will be studied in a future work.

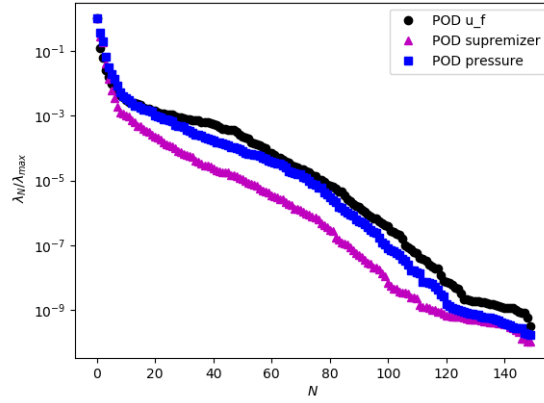


FIGURE 5. Steady case: POD eigenvalues decay for the fluid velocity \mathbf{u} (black), the fluid pressure p (blue), and the fluid supremizer \mathbf{s} (magenta), for a set of $N_{train} = 150$ snapshots.

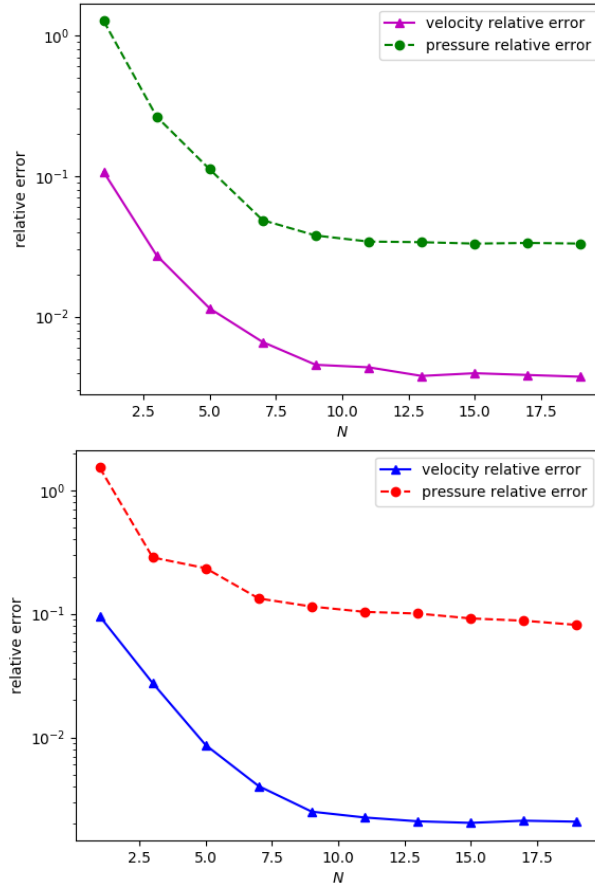


FIGURE 6. Steady case: Mode dependent errors between high fidelity and reduced order approximation, with (left) and without (right) the supremizer enrichment.

4.2. Unsteady Navier–Stokes with stationary in time geometry. In this paragraph we present the results obtained by applying the proposed reduction technique to a time dependent case. The time-step used in our simulation is $\tau = 0.011s$, and the final time is $T = 0.7s$. The fluid viscosity is $\nu_f = 0.05 \text{ cm}^2/s$ and the fluid density is $\rho_f = 1 \text{ g/cm}^3$. We impose a constant

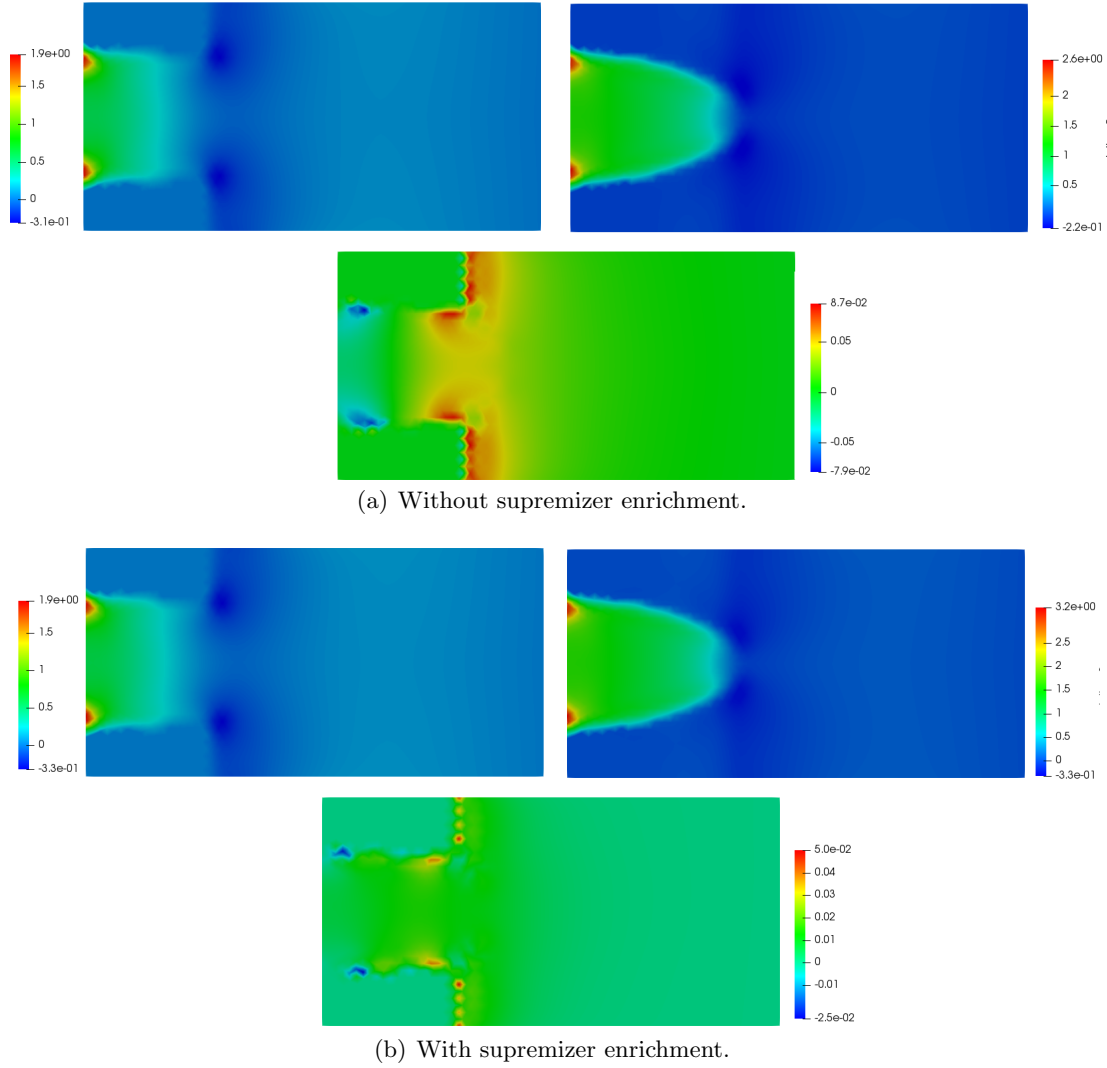
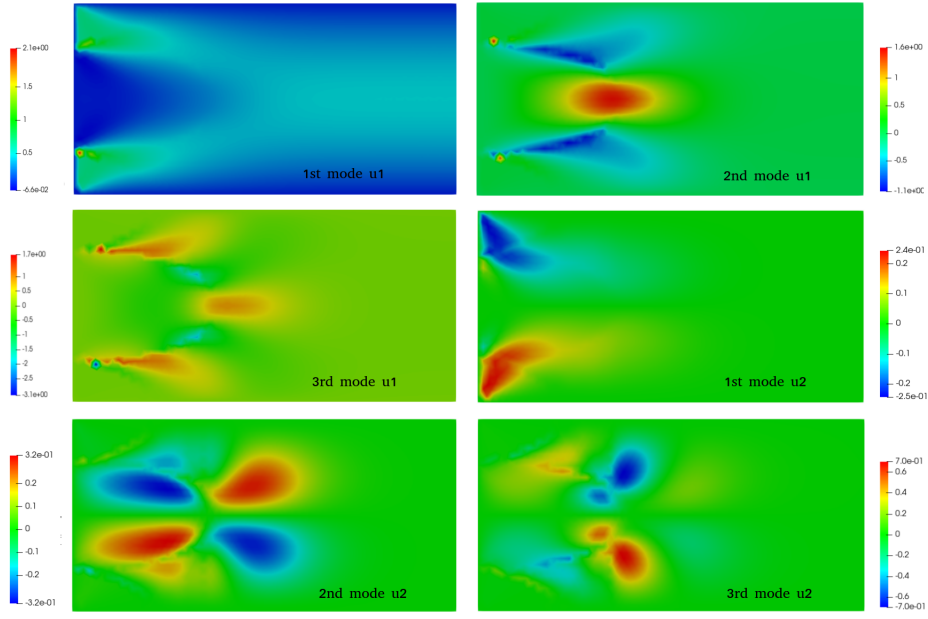


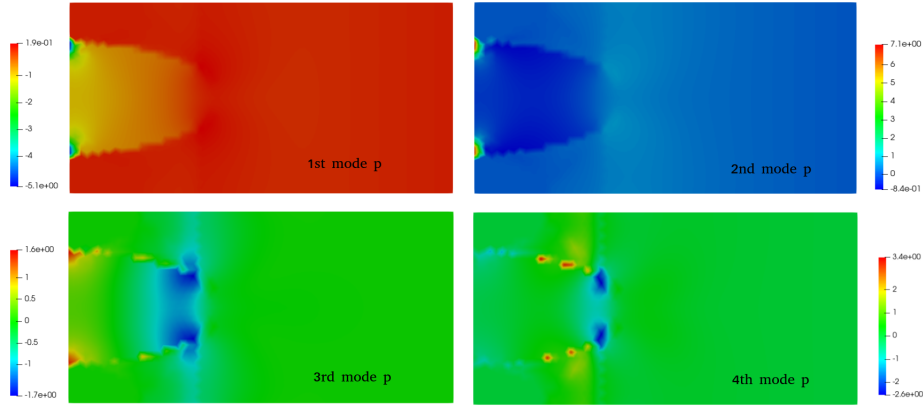
FIGURE 7. Steady case: Uncut geometry and the high fidelity pressure solution for parameter $\theta = -0.015854$ (left), reduced order solution for the same θ (right) and approximation error (middle)

inlet velocity $\mathbf{u}_{\text{in}} = (1, 0)$, and we impose a homogeneous boundary condition for the vertical component of the fluid velocity at the top and bottom walls of the rectangle. We now take $N_{\text{train}} = 200$, and we generate randomly N_{train} uniformly distributed values for the parameter θ . We also remind that we sample the time interval $[0, T]$ with an equispaced sampling $\{t_0, \dots, t_{N_t}\}$. We then run a POD on the set of snapshots collected, and we obtain our basis functions with which we are going to compute the reduced solutions $(\mathbf{u}_N(t, \theta_i), p_N(t, \theta_i))$, where $i = 1, \dots, N_{\text{test}}$, and N is the number of basis functions that we use. Figures 8 gives an example of the first modes that we obtain with this procedure, whereas in Figure 9 we show the rate of decay of the eigenvalues for all the components of the solution and for the supremizer. To test the reduced order model we generate randomly $N_{\text{test}} = 30$ uniformly distributed values for $\theta \in \mathcal{P}_{\text{test}}$.

We are again interested in the behavior of the relative approximation error as a function of the number N of basis functions used at the reduced order level. We therefore let N vary in a discrete set \mathcal{N} : for a fixed value of $N \in \mathcal{N}$, and for each θ_i , $i = 1, \dots, N_{\text{test}}$, we compute both the reduced solution $(\mathbf{u}_N(t, \theta_i), p_N(t, \theta_i))$ and the corresponding high order solution $(\mathbf{u}_h(t, \theta_i), p_h(t, \theta_i))$. We calculate the L^2 relative error $\epsilon_{u, t_k}^{N, i}$ for the velocity and the



(a) First six modes for the velocity.



(b) First four modes for the pressure.

FIGURE 8. Unsteady system with static in time geometry: Some reduced basis modes for velocity and pressure for the evolutionary in time, geometrically patrametrized Navier–Stokes system.

relative error $\epsilon_{p,t_k}^{N,i}$ for the pressure at time t_k , by taking an average of these relatives error we obtain the mean approximation error $\epsilon_u^{N,i}$ for \mathbf{u} and $\epsilon_p^{N,i}$ for p , for each $\theta_i \in \mathcal{P}_{\text{test}}$. Finally we compute the average approximation errors $\bar{\epsilon}_u^N$ and $\bar{\epsilon}_p^N$ for every $N \in \mathcal{N}$, defined as:

$$\bar{\epsilon}_u^N = \frac{1}{N_{\text{test}}} \sum_{i=1}^{N_{\text{test}}} \epsilon_u^{N,i}.$$

Figure 10 shows the relative approximation errors plotted against the number N of basis functions used, with and without of the supremizer enrichment at the reduced order level, respectively. As we can see, using a supremizer enrichment at the reduced level allows us to obtain a better approximation of the pressure: for example with $N = 40$ basis functions we have an approximation error $\bar{\epsilon}_p^N$ that is almost one order of magnitude smaller with respect of the approximation error that we obtain without the supremizer enrichment.

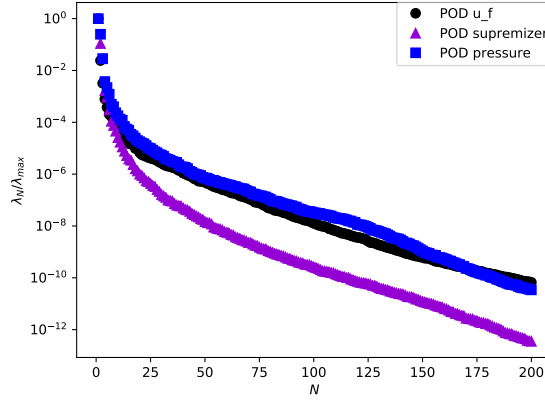


FIGURE 9. Time dependent case an the POD eigenvalues decay for the fluid velocity \mathbf{u} (black), the fluid pressure p (blue), and the fluid supremizer \mathbf{s} (magenta), for a set of $N_{train} = 200$ snapshots.

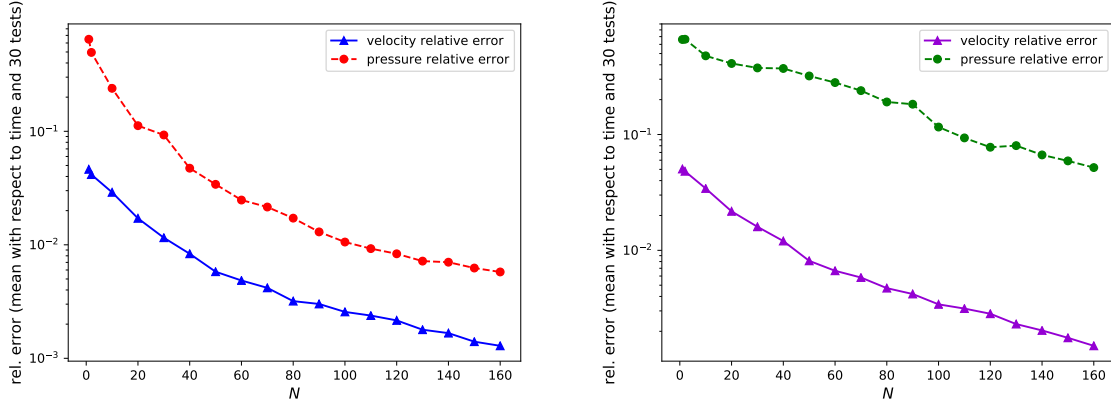


FIGURE 10. Unsteady case: Mode dependent errors between high fidelity and reduced order approximation, with and without the supremizer enrichment.

Figure 11(a) shows the approximation error for the pressure, for a given value of the test parameter θ , without the supremizer enrichment; the error has been calculated in the L^2 norm. Figure 11(b) shows the approximation error for the pressure, for the same parameter value, with the supremizer enrichment: as we can see, by employing a supremizer enrichment, we obtain a much more accurate approximation of the reduced order pressure. Figure 12 shows the approximation error for the fluid velocity \mathbf{u}_f for a given value of the test parameter θ , at the final time-step of the simulation.

4.3. Unsteady Navier–Stokes with evolutionary in time geometry. In this subsection we present the results obtained by applying the proposed reduction technique to a time dependent case, with evolutionary in time level set geometry. The values of the quantities that determine the oscillatory motion of the cylinder immersed in the fluid are reported in Table 3. The time-step used in our simulation is $\tau = 0.011s$, and the final time is $T = 400\tau = 4.4s$. Similarly to paragraph 4.2, we take the fluid viscosity $\nu_f = 0.05 \text{ cm}^2/s$, the fluid density $\rho_f = 1 \text{ g/cm}^3$, inlet velocity $\mathbf{u}_{in} = (1, 0)$ and the same boundary conditions. We choose $N_{train} = N_t = 400$ time instances, and we run a POD on the set of the collected snapshots, and we obtain our basis functions with which we are going to compute the reduced solutions $(\mathbf{u}_N(t^i, \theta^i), p_N(t^i, \theta^i))$, where $i = 1, \dots, N_t$, and N is the number of basis functions that we

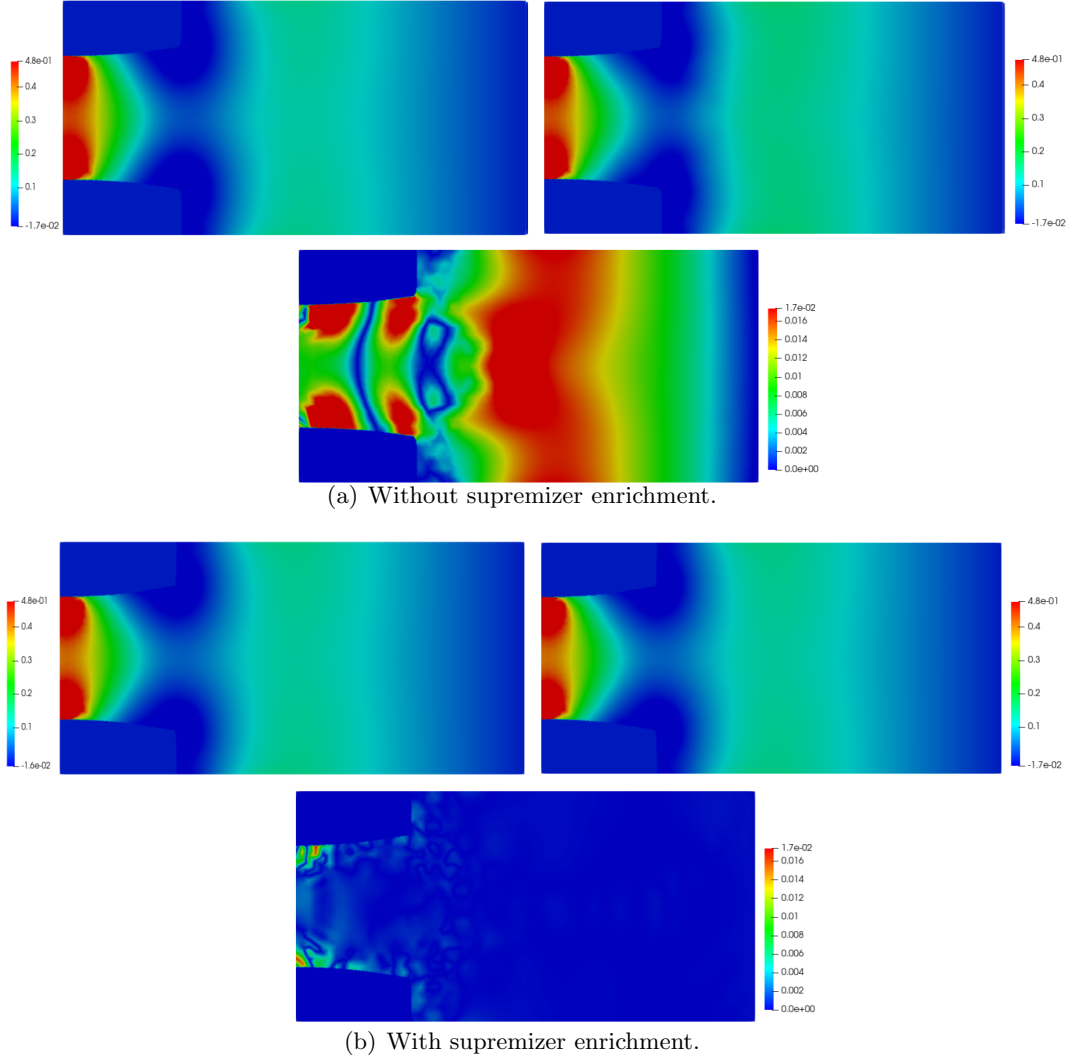


FIGURE 11. Unsteady case: Cut geometry and the high fidelity pressure solution at final time at final time $T = 0.7$ for parameter $\theta = 0.050014$ (left), reduced order solution for the same θ (right) and approximation error (bottom).

TABLE 3. Values for the parameters in the equation (7) of motion of the cylinder .

Parameter	Value
$\theta(0)$	$(-1.5, 0.25)$
A	0.015625
$\mu(t)$	$\left(\frac{\mu_{MAX} - \mu_{MIN}}{T}\right)t + \mu_{MIN}$
μ_{MAX}	0.5
μ_{MIN}	-0.5

use. Figures 13 represent some of the first modes that are derived with the POD procedure, while in Figure 14 we show the rate of decay of the eigenvalues for the velocity, pressure snapshot solutions and for the supremizer. Finally, we are interested in the behavior of the relative approximation error as a function of the number N of basis functions used at the reduced solution stage. We again let N vary in a discrete set \mathcal{N} : for a fixed value of $N \in \mathcal{N}$,

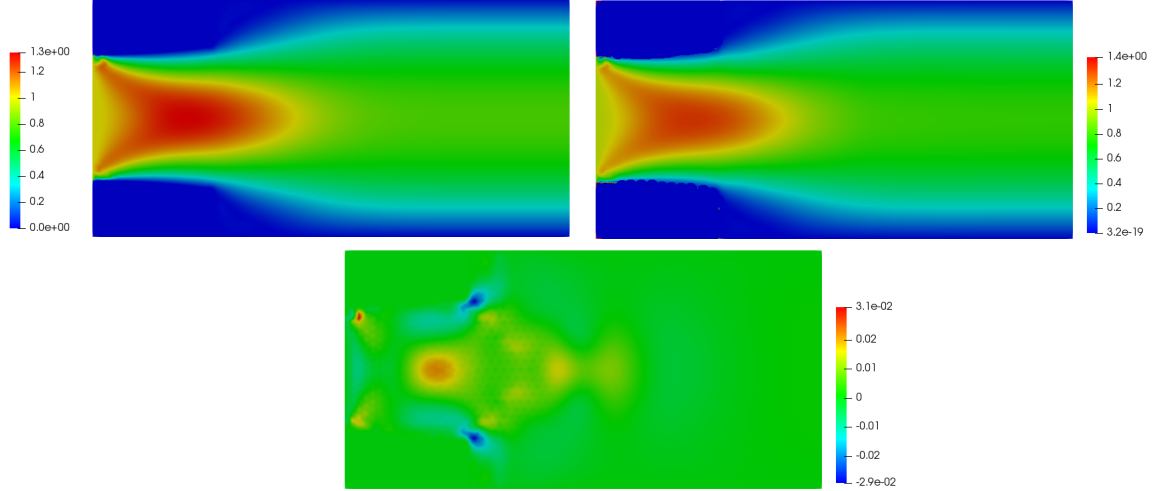


FIGURE 12. Unsteady case: Cut geometry and high fidelity fluid velocity at final time $T = 0.7$ for parameter $\theta = 0.045406$ (left), reduced order solution for the same θ (right) and approximation error (bottom).

and for each θ^i , $i = 1, \dots, N_t$, we compute both the reduced solution $(\mathbf{u}_N(t^i, \theta^i), p_N(t^i, \theta^i))$ and the corresponding high fidelity solution $(\mathbf{u}_h(t^i, \theta^i), p_h(t^i, \theta^i))$. We compute the L^2 relative error $\epsilon_{u,t_k}^{N,i}$ for the velocity and the relative error $\epsilon_{p,t_k}^{N,i}$ for the pressure at time t_k ; by taking the time average of these relative errors we obtain the mean approximation error $\epsilon_u^{N,i}$ for \mathbf{u} and $\epsilon_p^{N,i}$ for p , for each $\theta^i \in \mathcal{P}_t$.

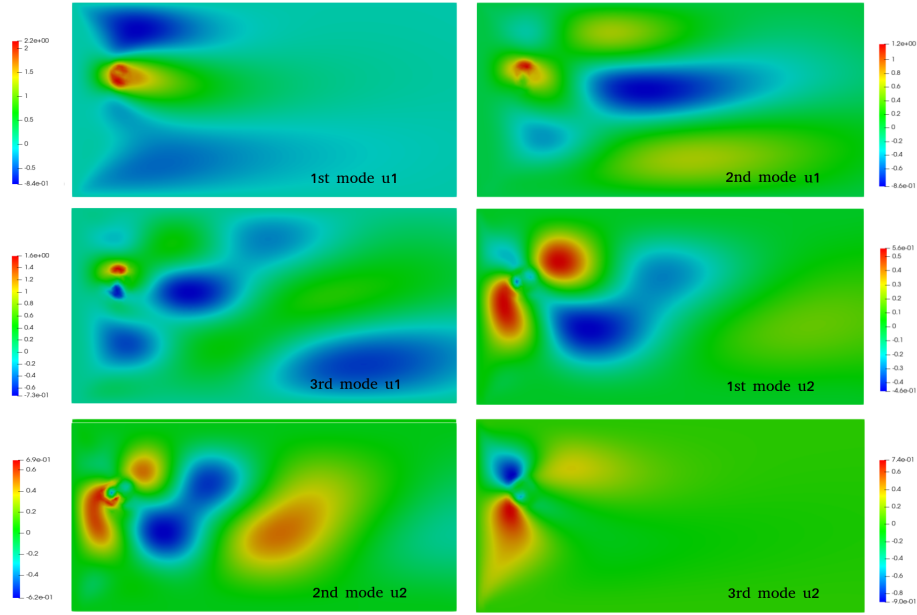
Figures 16 and 17 visualizes the approximation error for the pressure, at final time T , with supremizer enrichment as well as the velocity error; the error has been calculated in the L^2 norm. In Figure 15 the mean with respect time relative errors for various number of modes are visualized.

With this test case we can appreciate deeply the advantage that we obtain by employing the cutFEM reduced order model that we proposed. Indeed, at every new timestep t^i corresponds a different domain configuration, depending on the parameter θ^i ; without a cutFEM formulation, we would have to remesh at every timestep, making the offline phase of a reduced order model prohibitive from the computational cost point of view. Moreover, results show that we are able to obtain good results at the reduced order level even without employing a snapshot transportation during the offline phase.

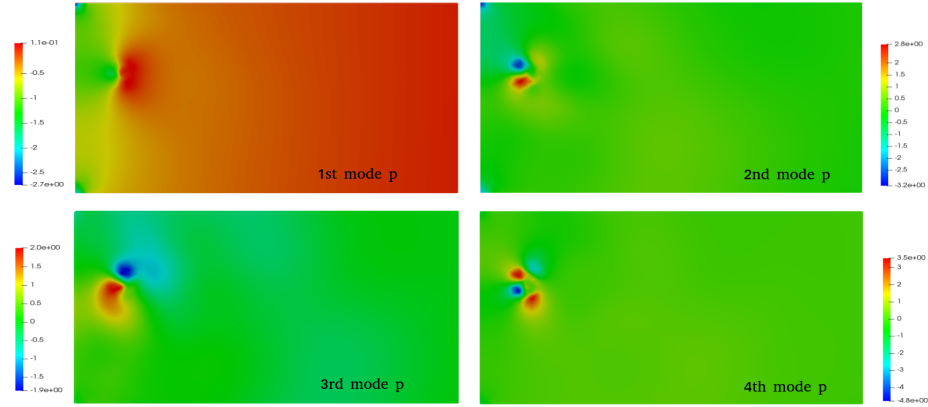
5. CONCLUSIONS

In this work we have introduced a POD–Galerkin ROM approach for geometrically parametrized two dimensional Navier–Stokes equations, both in the steady and in the unsteady case. We further extended the study to a problem where the levelset geometry changes in time, thus laying the basis for a future work on the application of ROMs based on CutFEM to Fluid–Structure Interaction problems. The procedure that we have proposed shows many of the advantages that characterize CutFEM and reduced order methods. First of all, by choosing an unfitted mesh approach, we have shown that it is possible to work with geometries that can potentially change significantly the shape of (part of) the domain, as we can see from the examples in Figure 1. By employing an unfitted CutFEM approach at the full order level, we can let the geometrical parameter θ vary in a large interval of values: this helps to overcome one of the limitations of the standard Finite Element discretization, where a re–meshing would have been needed.

At the reduced order level, we have extended the supremizer enrichment technique, widely used in the reduced basis community, to a CutFEM setting: the results that we have obtained



(a) First six modes for the velocity.



(b) First four modes for the pressure.

FIGURE 13. Unsteady system with evolutionary in time geometry: Some reduced basis modes for velocity and pressure for the evolutionary in time Navier–Stokes system.

confirm that the supremizer does actually significantly help in obtaining more accurate approximation of the fluid pressure allowing an inf-sup stable reduced basis preserving the stabilization effects. To conclude, with this work we started to prepare the basis for a CutFEM-RB procedure that, thanks to a Galerkin projection and with the use of a supremizer enrichment, will ideally be used to obtain accurate approximations of solutions of very complex problems, such as fully coupled multiphysics problem, where large displacements occur. Therefore, as future perspectives, we would like to test the performance of this approach with time dependent Fluid–Structure Interaction problems, geometrically shallow water flows as well as with phase flow Navier–Stokes systems. Furthermore, from the model reduction point of view, we will pursue further developments in hyper-reduction techniques [8, 13, 43, 45] tailored for unfitted discretizations.

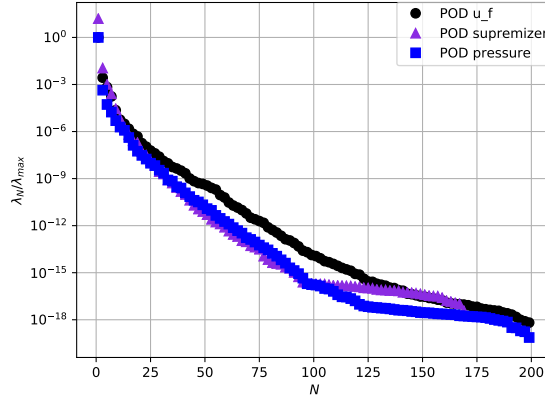


FIGURE 14. Evolutionary in time geometry: The POD eigenvalues decay for the fluid velocity \mathbf{u} (black), the fluid pressure p (blue), and the fluid supremizer \mathbf{s} (magenta), for a set of $N_{train} = N_t = 400$ (time instances) snapshots.

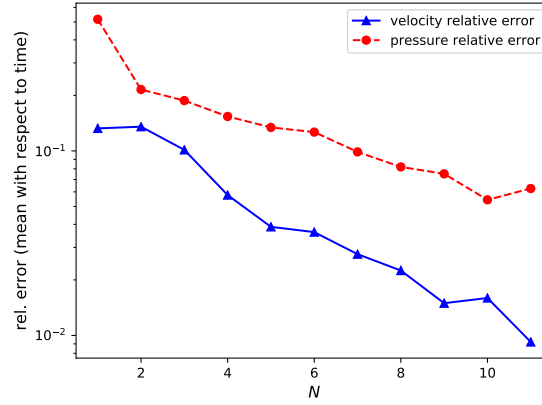


FIGURE 15. Evolutionary in time geometry: Mode dependent errors between high fidelity and reduced order approximation, with the supremizer enrichment.

ACKNOWLEDGEMENTS

We acknowledge the support by European Union Funding for Research and Innovation – Horizon 2020 Program – in the framework of European Research Council Executive Agency: Consolidator Grant H2020 ERC CoG 2015 AROMA-CFD project 681447 “Advanced Reduced Order Methods with Applications in Computational Fluid Dynamics” (PI Prof. Gianluigi Rozza). We also acknowledge the INDAM-GNCS project “Tecniche Numeriche Avanzate per Applicazioni Industriali”. The first author has received funding from the Hellenic Foundation for Research and Innovation (HFRI) and the General Secretariat for Research and Technology (GSRT), under grant agreement No[1115] and the National Infrastructures for Research and Technology S.A. (GRNET S.A.) in the National HPC facility - ARIS - under project ID pa190902. Numerical simulations have been obtained with the extension *ngsxfem* of *ngsolve* [1,3,38] for the high fidelity part, and RBniCS [2] for the reduced order part. We acknowledge developers and contributors of each of the aforementioned libraries.

REFERENCES

1. *ngsxfem* – Add-On to NGSolve for unfitted finite element discretizations, <https://github.com/ngsxfem/ngsxfem>.
2. *RBniCS* - reduced order modelling in FEniCS, <http://mathlab.sissa.it/rbnics>, 2015.

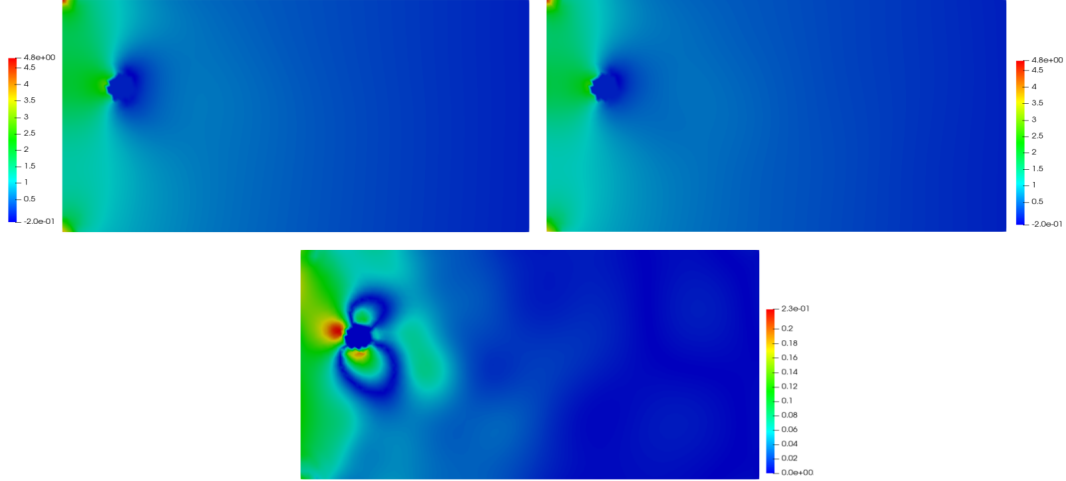


FIGURE 16. Unsteady case with evolutionary in time geometry: The high fidelity pressure solution at final time $t = T = 400\tau$ (left), reduced order solution for the same t (right) and approximation error (bottom). The results have been calculated with supremizer enrichment.

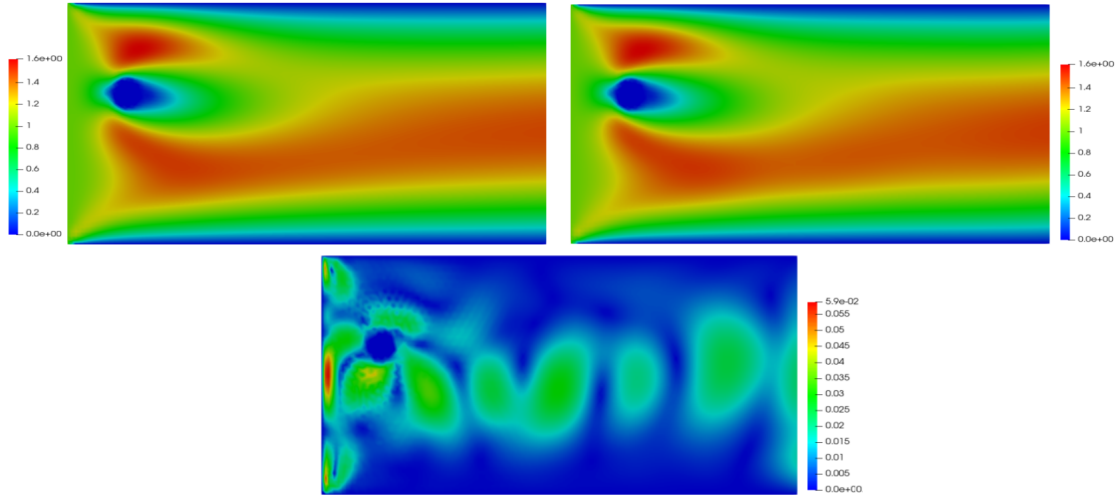


FIGURE 17. Unsteady case with evolutionary in time geometry: The high fidelity fluid velocity at final time $t = T = 400\tau$ (left), reduced order solution for the same t (right) and approximation error (bottom). The results have been calculated with supremizer enrichment.

3. *NGSolve - high performance multiphysics finite element software*, <https://github.com/NGSolve/ngsolve>, 2018.
4. *Projection-based reduced order models for a cut finite element method in parametrized domains*, *Computers & Mathematics with Applications* **79** (2020), no. 3, 833 – 851.
5. I. Akhtar, A. Nayfeh, and C. Ribbens, *On the stability and extension of reduced-order Galerkin models in incompressible flows*, *Theoretical and Computational Fluid Dynamics* **23** (2009), no. 3, 213–237.
6. M. Balajewicz and C. Farhat, *Reduction of nonlinear embedded boundary models for problems with evolving interfaces*, *Journal of Computational Physics* **274** (2014), 489–504.
7. F. Ballarin, A. Manzoni, A. Quarteroni, and G. Rozza, *Supremizer stabilization of POD-Galerkin approximation of parametrized steady incompressible Navier–Stokes equations*, *International Journal for Numerical Methods in Engineering* **102** (2015), no. 5, 1136–1161.

8. M. Barrault, Y. Maday, N. Nguyen, and A. Patera, *An ‘empirical interpolation’ method: application to efficient reduced-basis discretization of partial differential equations*, *Comptes Rendus Mathematique* **339** (2004), no. 9, 667–672.
9. P. Benner, M. Ohlberger, A. Patera, G. Rozza, and K. Urban, *Model Reduction of Parametrized Systems*, MS&A series, vol. 17, Springer, 2017.
10. M. Bergmann, C.-H. Bruneau, and A. Iollo, *Enablers for robust POD models*, *Journal of Computational Physics* **228** (2009), no. 2, 516–538.
11. E. Burman, S. Claus, P. Hansbo, M. Larson, and A. Massing, *CutFEM: discretizing geometry and partial differential equations*, *International Journal for Numerical Methods in Engineering* **104** (2014), 472–501.
12. A. Caiazzo, T. Iliescu, V. John, and S. Schyschlowa, *A numerical investigation of velocity-pressure reduced order models for incompressible flows*, *Journal of Computational Physics* **259** (2014), 598–616.
13. K. Carlberg, C. Farhat, J. Cortial, and D. Amsellem, *The GNAT method for nonlinear model reduction: Effective implementation and application to computational fluid dynamics and turbulent flows*, *Journal of Computational Physics* **242** (2013), 623 – 647.
14. F. Chinesta, A. Huerta, G. Rozza, and K. Willcox, ch. *Model Reduction Methods*, pp. 1–36, John Wiley & Sons, 2017.
15. F. Chinesta, P. Ladeveze, and E. Cueto, *A Short Review on Model Order Reduction Based on Proper Generalized Decomposition*, *Archives of Computational Methods in Engineering* **18** (2011), no. 4, 395.
16. A. Dumon, C. Allery, and A. Ammar, *Proper general decomposition (PGD) for the resolution of Navier–Stokes equations*, *Journal of Computational Physics* **230** (2011), no. 4, 1387–1407.
17. L. Fick, Y. Maday, A. Patera, and T. Taddei, *A Reduced Basis Technique for Long-Time Unsteady Turbulent Flows*, arXiv preprint arXiv:1710.03569, 2017.
18. A. Gerner and K. Veroy, *Certified Reduced Basis Methods for Parametrized Saddle Point Problems*, *SIAM Journal on Scientific Computing* **34** (2012), no. 5, A2812–A2836.
19. M. Grepl, Y. Maday, N. Nguyen, and A. Patera, *Efficient reduced-basis treatment of nonaffine and nonlinear partial differential equations*, *ESAIM: M2AN* **41** (2007), no. 3, 575–605.
20. M. Grepl and A. Patera, *A posteriori error bounds for reduced-basis approximations of parametrized parabolic partial differential equations*, *ESAIM: M2AN* **39** (2005), no. 1, 157–181.
21. B. Haasdonk and M. Ohlberger, *Efficient reduced models and a posteriori error estimation for parametrized dynamical systems by offline/online decomposition*, *Mathematical and Computer Modelling of Dynamical Systems* **17** (2011), no. 2, 145–161.
22. J. Hesthaven, G. Rozza, and B. Stamm, *Certified Reduced Basis Methods for Parametrized Partial Differential Equations*, SpringerBriefs in Mathematics, Springer International Publishing, 2016.
23. T. J. R. Hughes, G. Scovazzi, and L. P. Franca, *Multiscale and stabilized methods*, pp. 1–64, John Wiley & Sons, 2017.
24. A. Iollo, S. Lanteri, and J.-A. Désidéri, *Stability Properties of POD–Galerkin Approximations for the Compressible Navier–Stokes Equations*, *Theoretical and Computational Fluid Dynamics* **13** (2000), no. 6, 377–396.
25. I. Kalashnikova and M. F. Barone, *On the stability and convergence of a Galerkin reduced order model (ROM) of compressible flow with solid wall and far-field boundary treatment*, *International Journal for Numerical Methods in Engineering* **83** (2010), no. 10, 1345–1375.
26. E. Karatzas and G. Rozza, *Reduced Order Modeling and a stable embedded boundary parametrised Cahn–Hilliard phase field system based on cut finite elements*, In preparation, 2020.
27. E. Karatzas, G. Stabile, L. Nouveau, G. Scovazzi, and G. Rozza, *A reduced basis approach for PDEs on parametrized geometries based on the shifted boundary finite element method and application to a Stokes flow*, *Computer Methods in Applied Mechanics and Engineering* **347** (2019), 568 – 587.
28. E. Karatzas, G. Stabile, L. Nouveau, G. Scovazzi, and G. Rozza, *A Reduced-Order Shifted Boundary Method for Parametrized Incompressible Navier–Stokes Equations*, Submitted, 2020.
29. E. N. Karatzas, G. Stabile, N. Atallah, G. Scovazzi, and G. Rozza, *A Reduced Order Approach for the Embedded Shifted Boundary FEM and a heat exchange system on parametrized geometries*, IUTAM Symposium on Model Order Reduction of Coupled Systems, Stuttgart, Germany, May 22–25, 2018 (Cham), Springer International Publishing, 2020, pp. 111–125.
30. K. Kunisch and S. Volkwein, *Galerkin proper orthogonal decomposition methods for a general equation in fluid dynamics*, *SIAM Journal on Numerical Analysis* **40** (2002), no. 2, 492–515.
31. A. Quarteroni, A. Manzoni, and F. Negri, *Reduced basis methods for partial differential equations*, vol. 92, UNITEXT/La Matematica per il 3+2 book series, Springer International Publishing, 2016.
32. A. Quarteroni and G. Rozza, *Numerical solution of parametrized Navier–Stokes equations by reduced basis methods*, *Numerical Methods for Partial Differential Equations* **23** (2007), no. 4, 923–948.
33. A. Rokhzadi, *IMEX and Semi-Implicit Runge-Kutta Schemes for CFD Simulations*, Ph.D. thesis, Civil Engineering Department, Faculty of Engineering, University of Ottawa, 2018.

34. G. Rozza, D. Huynh, and A. Patera, *Reduced basis approximation and a posteriori error estimation for affinely parametrized elliptic coercive partial differential equations: Application to transport and continuum mechanics*, Archives of Computational Methods in Engineering **15** (2008), no. 3, 229–275.
35. G. Rozza, D. B. P. Huynh, and A. Manzoni, *Reduced basis approximation and a posteriori error estimation for Stokes flows in parametrized geometries: Roles of the inf-sup stability constants*, Numerische Mathematik **125** (2013), no. 1, 115–152.
36. G. Rozza, D. B. P. Huynh, and A. T. Patera, *Reduced basis approximation and a posteriori error estimation for affinely parametrized elliptic coercive partial differential equations*, Arch. Comput. Meth. Eng. **15** (2008), 229–275.
37. G. Rozza and K. Veroy, *On the stability of the reduced basis method for Stokes equations in parametrized domains*, Computer Methods in Applied Mechanics and Engineering **196** (2007), no. 7, 1244–1260.
38. J. Schöberl, *C++11 implementation of finite elements in NGSolve*, Institute for Analysis and Scientific Computing, Vienna University of Technology (2014).
39. S. Sirisup and G. Karniadakis, *Stability and accuracy of periodic flow solutions obtained by a POD-penalty method*, Physica D: Nonlinear Phenomena **202** (2005), no. 3-4, 218–237.
40. G. Stabile, F. Ballarin, G. Zuccarino, and G. Rozza, *A reduced order variational multiscale approach for turbulent flows*, Advances in Computational Mathematics (2019), 1–20.
41. G. Stabile, S. Hijazi, A. Mola, S. Lorenzi, and G. Rozza, *POD-Galerkin reduced order methods for CFD using Finite Volume Discretisation: vortex shedding around a circular cylinder*, Communications in Applied and Industrial Mathematics **8** (2017), no. 1, 210 – 236.
42. G. Stabile and G. Rozza, *Finite volume POD-Galerkin stabilised reduced order methods for the parametrised incompressible Navier-Stokes equations*, Computers & Fluids **173** (2018), 273–284.
43. G. Stabile, M. Zancanaro, and G. Rozza, *Efficient geometrical parametrization for finite-volume-based reduced order methods*, International Journal for Numerical Methods in Engineering **121** (2020), no. 12, 2655–2682.
44. K. Veroy, C. Prud’homme, and A. Patera, *Reduced-basis approximation of the viscous Burgers equation: rigorous a posteriori error bounds*, Comptes Rendus Mathématique **337** (2003), no. 9, 619–624.
45. D. Xiao, F. F., A. Buchan, C. Pain, I. Navon, J. Du, and G. Hu, *Non linear model reduction for the Navier–Stokes equations using residual DEIM method*, Journal of Computational Physics **263** (2014), 1–18.